CHEMISTRY OF MATERIALS
Review

Chem. Mater. **2011,** *23,* 359–377 359
DOI:10.1021/cm1021257

Design of Organic Semiconductors from Molecular Electrostatics†

Georg Heimel,*,‡ Ingo Salzmann,‡ Steffen Duhm,§ and Norbert Koch‡

‡*Institut für Physik, Humboldt-Universität zu Berlin, Brook-Taylor-Strasse 6, D-12489 Berlin, Germany, and* §*Graduate School of Advanced Integration Science, Chiba University, 1-33 Yayoi-cho, Inage-ku, Chiba 263-8522, Japan*

Received July 29, 2010. Revised Manuscript Received September 20, 2010

Progress in the field of organic electronics depends on the synthesis of new π-conjugated molecules to further improve the performance of, for example, organic light-emitting diodes, organic photovoltaic cells, and organic field-effect transistors. However, the interrelation between the properties of isolated molecules on one hand and close-packed thin films on the other hand is far from trivial. Here, we review recent progress in the understanding of electrostatic phenomena, which originate in the collective action of the anisotropic charge distribution in typical conjugated molecules. Both the π-electron systems and polar end-group substitutions exposed at the surface of a molecular or polymeric film are seen to form dipole layers, which critically impact the device-relevant ionization energy and electron affinity of that film. After briefly revisiting electrostatic fundamentals and critically assessing related experimental methods, the energies of the frontier electronic states in organic thin films are shown to depend appreciably on the orientation of the constituent molecules with respect to device-relevant interfaces. For films of preferentially "standing" or "edge-on" molecules, this opens the possibility for electronic-structure engineering with intramolecular polar bonds. On the basis of these findings, additional insights into the working principles of organic electronic devices are provided and valuable guidelines for the synthesis of improved organic semiconductors are derived.

1. Introduction

The overarching vision in the field of organic electronics is the realization of flexible,[1−3] easy-to-process,[4−9] and low-cost (opto)electronic devices[10−12] such as organic light-emitting diodes (OLEDs) for large-area display and lighting applications,[13−19] organic photovoltaic cells (OPVCs),[20−25] and organic field-effect transistors (OFETs),[26−33] where the active layer(s) are composed of semiconducting small organic molecules or polymers. The rich chemistry of π-conjugated (macro)molecules promises that the materials properties of organic semiconductors can be readily tuned toward application-specific demands. Therefore, the entire field is quintessentially synthetic chemistry driven, and new compounds, expected to lead to improvements in device performance, appear at a steady if not increasing rate. Not always, however, is the anticipated improvement in device performance observed. Therefore, the community has adopted a multidisciplinary effort, which drives truly knowledge-based progress by combining the complementary competences of electrical engineering, materials science and engineering, physics, and chemistry. Ideally, these disciplines work together in a concerted effort to (a) carefully collect and critically evaluate device data, (b) reliably identify limiting factors, and (c) formulate requirements for molecular structures, which can then be fed back into synthesis.

Already (b) poses formidable challenges, as precise control over both device structure and parameters is required together with a mature understanding of the device physics and the physics of defect-rich organic semiconductors. One limiting factor, however, has been clearly identified: The energy-level alignment at the ubiquitous materials interfaces in organic (opto)electronic devices.[34−44] At organic/organic heterojunctions, the energy offset between the frontier electronic levels of two materials, that is, their respective ionization energies and electron affinities, impacts charge-carrier transport as well as the formation and diffusion of excitons (i.e., bound electron−hole pairs) in multilayer OLEDs, and exciton dissociation in OPVCs.[13,23,25,39−44] Likewise, the relative alignment between the ionization and affinity levels of an organic semiconductor with the Fermi level of a metallic contact governs charge-carrier injection in OLEDs and OFETs and affects the open-circuit voltage in OPVCs.[34−39]

As a starting point to address these issues, synthetic chemistry often focuses on the properties, specifically on the electronic structure, of *isolated* molecules. Consequently, also the analytic techniques employed to verify the achieved ionization energies and electron affinities are generally geared toward the determination of single-molecule properties. However, one has to bear in mind that the active component in organic electronic devices is usually a thin film, that is, an *ensemble* of tightly packed molecules or polymer chains. While it is clearly the ensemble properties that determine device performance,

† Accepted as part of the "Special Issue on π-Functional Materials".
*Corresponding author. E-mail: georg.heimel@physik.hu-berlin.de.

Published on Web 10/25/2010

their relation to single-molecule properties, that is, the transition from (b) to (c) as defined above, is far from trivial. For example, the interplay between molecular structure and ensuing solid-state packing, thin-film growth, and morphology is qualitatively understood at best.[45−51]

Here, we review recent progress in understanding the interrelation between thin-film electronic structure and the corresponding single-molecule properties. In particular, we discuss dipole layers present at surfaces of ordered molecular assemblies, which originate in the collective electrostatic action of the anisotropic electron distribution in individual constituent molecules or polymer chains. These intrinsic surface dipoles are shown to lead to a pronounced dependence of the ionization energy of organic layers on the orientation of the constituent molecules or polymer chains with respect to relevant surfaces or interfaces. Ultimately, purely electrostatic effects are seen to substantially—maybe even dominantly—affect the energy-level alignment at organic/(in)organic interfaces. This fundamental insight permits connecting thin-film electronic properties, the performance, and even the functionality of organic electronic devices to molecular structure. Thus closing the cycle for continuous development and improvement, valuable guidelines for the synthesis of organic semiconductors and device design can be derived.

2. Electrostatic Considerations

Prior to touching the core of the subject matter, it is useful to recall some basic concepts of electrostatics. In particular, the electrostatic potential created by isolated electric dipoles and quadrupoles as well as the corresponding two-dimensional (2D) charge distributions is briefly recapitulated. Rather than delving into a rigorous mathematical treatment, emphasis is put on a qualitative description of those characteristic features that are relevant for the purposes of this Review.

Figure 1a shows the electrostatic potential energy of an electron, E, in a plane through an electric dipole (see inset) consisting of two point charges $+0.1\ q_e$ (left) and $-0.1\ q_e$ (right) separated by $d = 2$ Å. Note that $E = -q_eV$, where V is the electrostatic potential and q_e denotes the (by definition positive) elementary charge. The two key qualitative features for the purposes of this Review are:

(i) Around the singularities at the locations of the point charges, the electron potential energy rapidly converges to one common value, namely, the vacuum level, E_{vac}.

(ii) Immediately to the left of the positive charge, E is lower, and immediately to the right of the negative charge, the electron potential energy is higher than E_{vac}.

Next, the specific quadrupolar arrangement of point charges shown in the inset of Figure 1b is considered. It consists of the linear charge sequence $-0.1\ q_e\,|\,+0.1\ q_e\,|\,+0.1\ q_e\,|\,-0.1q_e$, each separated by a distance of $d = 2$ Å. Comparison with Figure 1a reveals that this charge distribution can alternatively be regarded as two back-to-back dipoles pointing toward each other. Examination of the electron potential energy in a plane containing this linear quadrupole (Figure 1b) reveals that, again, E rapidly converges to one common value, E_{vac}, around the singularities at the locations of the point charges. The third key observation, however, is that

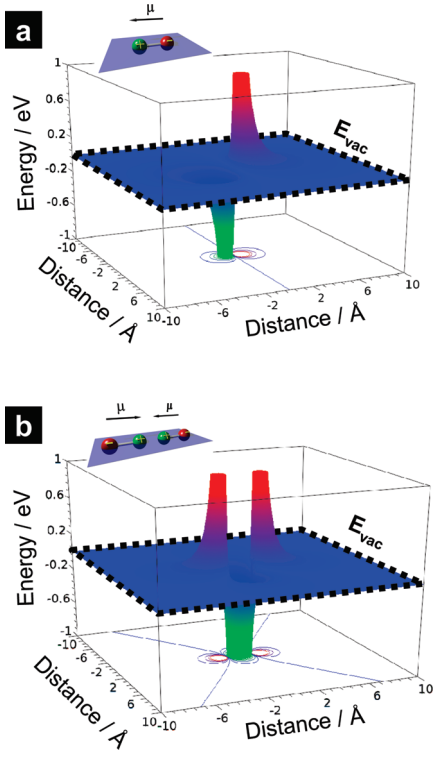

Figure 1. (a) The electrostatic potential energy for electrons in the plane of an electric dipole, μ, of point charges ($\pm^1/_{10}$ of the elementary charge) at a separation of 2 Å rapidly decays to the vacuum level, E_{vac}. (b) Electrostatic potential energy for electrons in the plane of a linear electric quadrupole of point charges ($\pm^1/_{10}$ of the elementary charge).

(iii) Immediately to the left of the leftmost (negative) charge and to the right of the rightmost (negative) charge, that is, "outside" the linear quadrupole, the electron potential energy is higher than E_{vac}, while it is lower on the "inside", that is, in the spatial region around and between the two central (positive) charges.

Increasing the dimensionality of the system, an infinitely extended 2D layer of discrete dipoles (schematic in Figure 2) is considered next. The electron potential energy in a plane cutting perpendicularly through such a layer is depicted in the three-dimensional (3D) plot in the right panel of Figure 2. Similarly to the isolated dipole discussed above, E is lower on the left (positive) side of the discrete dipole layer and higher on the right (negative) side. In stark contrast, however, the electron potential energy now rapidly converges to *different* values on either side of the double layer instead of converging to the *same* common value on both sides. This striking qualitative difference is of key importance and we note that, in general,

(iv) A dipole layer gives rise to a step in the electrostatic potential.

The magnitude of this potential-energy step, ΔE, is connected to the absolute value of the dipole moment, μ, per

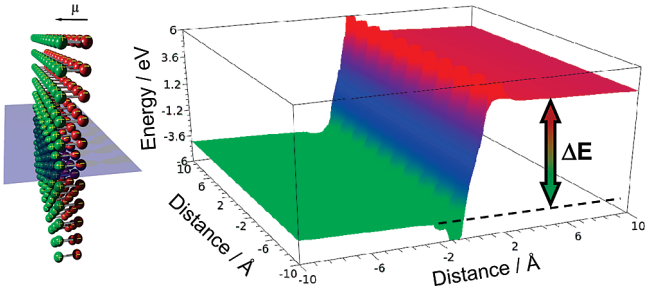

Figure 2. Electrostatic potential energy for electrons in a plane cutting through a layer of discrete dipoles ($\pm^1/_{10}$ of the elementary charge separated by 2 Å) that are laterally spaced by 2 Å on a square grid. The magnitude of the potential-energy step is indicated by ΔE.

surface area, A, through the Helmholtz equation. Recalling that μ is given by the amount of separated charge, q, multiplied by the separation distance, d, this equation reads:

$$\Delta E = \frac{\mu}{\varepsilon_0 A} = \frac{q \cdot d}{\varepsilon_0 A} \qquad (1)$$

where ε_0 denotes the vacuum permittivity. Consistent with the situation in Figure 1, the points in Figure 2 carry a charge of $\pm 0.1\ q_e$. As they are laterally separated by $a = 2$ Å on a square grid, the relevant area A is 4 Å^2. Like in Figure 1a, layers of oppositely charged points are separated by $d = 2$ Å in the direction perpendicular to the layer resulting in a dipole area density of 0.1 q_e times 2 Å per 4 Å^2, which amounts to 0.05 q_eÅ^{-1}. Division by ε_0 finally yields a potential-energy step of $\Delta E \approx 9$ eV.

Another noteworthy detail apparent in Figure 2 is that the spatial inhomogeneities in the electrostatic potential, caused by the singularities at the locations of the point charges, rapidly decay outside the discrete dipole layer. More precisely, the characteristic decay length in such a case is $a/2\pi$.[52] Outside this range, the potential is essentially constant on either side of the discrete dipole layer (analogously to a plate capacitor). In other words,

(v) Fluctuations in the electrostatic potential energy due to lateral inhomogeneities within the charge distribution constituting a dipole layer decay on a length scale comparable to the in-plane distances characterizing these inhomogeneities.

This observation justifies further simplifying the situation by replacing the layer of discrete dipoles with an infinitely extended 2D dipole layer consisting of two homogenously charged slabs (inset in Figure 3a). Assuming an area charge of $\pm 0.05\ q_e$Å^{-2} and a thickness of 1 Å for each slab, the electron potential energy along a line perpendicular to the dipole layer (blue arrow in inset) is plotted in Figure 3a. The same ΔE as in Figure 2 is observed with the difference that the potential energy is now exactly constant immediately outside the dipolar slab.

Clearly, dipole layers of *infinite* lateral extension are hardly relevant for real-world systems. The important qualitative differences between a single isolated dipole (Figure 1a) and a 2D dipole layer (Figures 2 and 3a) presage that the lateral extent of a dipolar charge distribution has important consequences for the induced

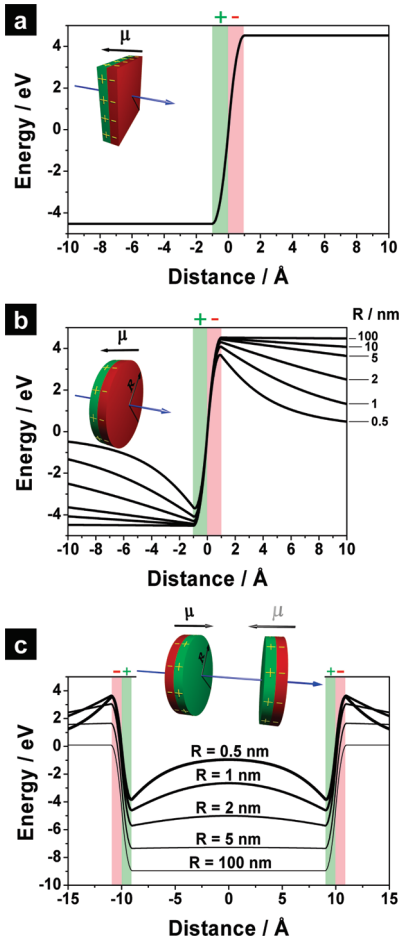

Figure 3. (a) Electrostatic potential energy for electrons across an infinite dipole layer of two 1 Å thick homogenously charged slabs ($\pm^1/_{20}$ of the elementary charge per Å^2). (b) Electrostatic potential energy for electrons along the symmetry axis of a dipole disk consisting of two 1 Å thick homogenously charged slabs ($\pm^1/_{20}$ of the elementary charge per Å^2) of radius R. (c) Electrostatic potential energy for electrons along the symmetry axis of two opposing dipole disks at a separation of 20 Å, each consisting of two 1 Å thick homogenously charged slabs ($\pm^1/_{20}$ of the elementary charge per Å^2) of radius R.

potential. Therefore, the case of finite-sized dipole layers is considered as a next step. Let us assume the representative example of two oppositely and homogenously charged disks (area charge $\pm 0.05\ q_e$Å^{-2}) of radius R and a thickness of 1 Å. The electron potential energy along the symmetry axis of the system (blue arrow in the schematic) is plotted in Figure 3b for different values of R.[34] Similarly to the isolated dipole (Figure 1a), E value on both sides of the dipolar disk converges to one common value of E_{vac} on a length scale comparable to the disk diameter. For large radii this implies that, although E still decays eventually, the situation is essentially identical to the case of an infinite dipole layer (Figure 3a), if one is interested only in the potential energy in the immediate vicinity of the dipolar disk, for example, within a few angstroms; there, E is essentially constant on either side but assumes different values. We note that

(vi) A finite dipole layer can still be regarded as infinite if its lateral extension is significantly larger than the distance from the layer where the electrostatic potential is sought.

Finally, the 2D analogue to the quadrupole shown in Figure 1b is considered, that is, two back-to-back dipole layers of finite lateral extent. Specifically, we assume two parallel dipolar disks (as the one discussed above) with opposing dipole moments pointing toward each other, that is, with their negative sides on the outside (see inset). For a distance of 20 Å between the disk centers, the electron potential energy along the symmetry axis of the system (blue arrow in the inset) is plotted in Figure 3c for a series of radii. For small R, the system strongly resembles an isolated quadrupole (Figure 1b). Although the electron potential energy is lower between the disks and higher directly outside the disks, it converges to one common value of E_{vac} on a length scale comparable to the diameter of the disks. However, for larger R (compared to typical distances characterizing the entire structure), a potential well of depth ΔE is found with constant values for E both between and outside the disks. The last key observation thus can be formulated as

(vii) The spatial region between two 2D dipole layers with opposing dipole moments pointing toward each other (i.e., negative on the outside) lies at a lower electron potential energy than the region both directly outside the dipole layers and the common E_{vac} far from the entire charge distribution.

3. From Molecules to Molecular Layers

We now apply the insight gained from recollecting some fundamental electrostatic aspects of representative model systems to the electrostatics of π-conjugated (and aromatic) molecules to highlight the important consequences for their electronic structure. In analogy to the preceding section, isolated species are treated first, followed by ordered 2D molecular monolayers, which can also be regarded as the outermost layer terminating the surface on an organic thin film or a molecular crystal.

3.1. π-System Dipole. As archetypical planar system with an extended π-electron system, the simplest aromatic molecule, benzene, is chosen. The π-electrons reside in molecular orbitals (MOs), which have a node in the plane of the molecule and extend into space on both sides (Figure 4a). In contrast, the charge distribution arising from the nuclei and the remaining (core- and σ-) electrons is centered in the molecular plane. The negatively charged π-electron clouds on both sides of the molecular plane are thus compensated by a net positive charge within the plane. As outlined in the preceding section, this particular arrangement of charges represents an electric quadrupole which, alternatively, can be regarded as two dipoles, μ_π, pointing toward each other. To further highlight the equivalence to the situation depicted in Figure 1b, density-functional theory (DFT) was employed to calculate the electron potential energy in a plane cutting perpendicularly through the molecule (Figure 4b). The result reveals regions of higher potential energy next to the π-electron clouds on both sides of the molecular plane, whereas regions of lower electrostatic potential are found in the plane of the molecule next to the hydrogen atoms (Figure 4c). Importantly, and

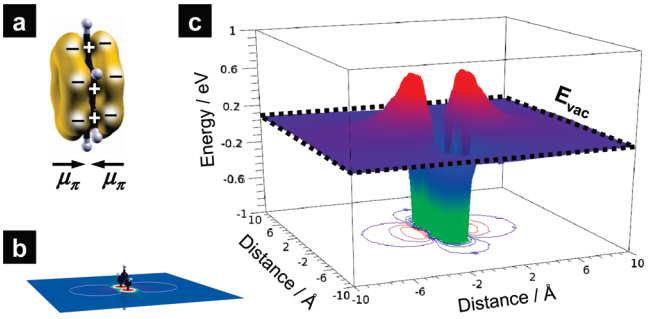

Figure 4. (a) Schematic of the electron distribution in a benzene molecule; the π-electron clouds on both sides of the molecule carry a negative charge, which is compensated by positive charges in the molecular plane, thus giving rise to two opposing dipoles, μ_π. (b) Plane through the molecule chosen for (c), where the electrostatic potential energy for electrons, as calculated by density-functional theory, is shown; a common vacuum level, E_{vac}, is established close to the isolated molecule.

again in full analogy to the point-charge model in Figure 1b, the potential around an isolated benzene molecule rapidly (i.e., within a few angstroms) converges to one common value of E_{vac}.

3.2. Introducing Energy Levels. To understand the consequences of molecular electrostatics for the observable molecular electronic structure, also the concepts of ionization energy, IE, and electron affinity, EA, need to be revisited in brief. The former is commonly understood as the energy required for removing one electron from the neutral molecule, and the latter is regarded as the energy gained by adding one electron to the neutral molecule. Importantly, however, these two quantities are, in fact, energy differences between a final and an initial state of the system. For IE, the energy of the initial state is that of the neutral molecule, E^0, and the final-state energy is that of the cation, E^+, plus E^∞_{vac}, the energy of a free electron at rest in vacuum infinitely far away from the charged molecule (eq 2a)

$$IE = (E^+ + E^\infty_{vac}) - E^0 \quad (2a)$$

$$-EA = E^- - (E^0 + E^\infty_{vac}) \quad (2b)$$

Conversely, for EA, the final-state energy is that of the anion, E^-, and the energy of the initial state is the sum of E^0 and E^∞_{vac}; to obtain positive numbers for EA, it is usually given as the negative of that energy difference (eq 2b). With Koopmans' theorem in mind,[53] the differences $(E^0 - E^+)$ and $(E^- - E^0)$ are often approximated by the energies of the highest occupied molecular orbital (HOMO) and the lowest unoccupied molecular orbital (LUMO), respectively.[54−58] This transforms eqs 2 into

$$IE = E^\infty_{vac} - E_{HOMO} \quad (3a)$$

$$-EA = E_{LUMO} - E^\infty_{vac} \quad (3b)$$

From Figure 4c it becomes apparent that a common E_{vac} is established much closer to the molecule (within a few angstroms) than infinity. As the origin of the potential-energy scale can be freely chosen, $E^\infty_{vac} = E_{vac}$ is commonly set to zero. Equations 3 then imply that a single isolated molecule has *one* and only one well-defined $IE \approx -E_{HOMO}$ and $EA \approx -E_{LUMO}$.

3.3. Intrinsic Surface Dipole Layers in π-Conjugated Materials. As the active components in organic (opto)electronic devices are, in fact, molecular thin films rather than single molecules, the line of thought introduced in section 2 can be pursued to derive the electrostatics of an ordered molecular monolayer from that of an isolated molecule. We emphasize that the reasoning below is equally valid for organic solids or thin films in general, which typically consist of many layers. In this case, the system discussed below is to be regarded as the outermost layer terminating that organic solid or thin film and molecules in consecutive layers are assumed to exhibit the same packing and orientation. As an important class of materials, the focus will first be on unsubstituted and planar conjugated molecules, for which benzene served as a model (*vide supra*). Depending on the preparation method, the growth conditions, and the type of substrate as well as its pretreatment,[59−70] two limiting cases for the orientation of such molecules with respect to the surface of an organic thin film are conceivable: one where the molecular planes are parallel to the surface, henceforth referred to as "lying", and the other with the molecular planes perpendicular to the surface, denoted as "standing" in the following.

As outlined in the preceding subsection, an isolated π-conjugated molecule can, in the context of electrostatics, be regarded as the equivalent to a linear quadrupole of point charges (compare Figures 4 and 1). The two opposing dipole disks in Figure 3c may portray the situation even more accurately, assuming small diameters (i.e., the approximate "diameter" of the molecule) and small separation (i.e., approximate "thickness" of the molecule). Assembling such molecules into a close-packed lying monolayer then corresponds to increasing the radius of the disks, the consequences of which are highlighted in Figure 3c. Note that lateral inhomogeneities in the electrostatic potential above such a layer (composed of individual molecules) decay on the length scale of intermolecular distances (i.e., a few angstroms) and, thus, need not be considered (Figure 2).[52] The effect of the potential trough (Figure 3c) on the energy levels within a layer of lying molecules is schematically depicted in Figure 5a. The nuclei together with the core- and σ-electrons create one part of the potential well for all electrons in the molecules (left panel). The quadrupolar electron distribution of the π-electrons (Figure 4) creates an additional potential trough of depth ΔE, that is, a region of lower potential energy centered on the molecular planes and regions of higher potential energy on both sides of the layer (center panel). The sum of these two contributions can be thought of as the actual potential well "felt" by electrons. Since the lateral extension of a molecular monolayer can never be infinite in practice, the higher potential on either side of the layer, E_{vac}, decays toward the vacuum level far from the sample, E^{∞}_{vac}, on the length scale of the layer radius (see Figure 3c).[34,71]

From the definition of *IE* (eq 3a) it becomes apparent that, in contrast to a single isolated molecule (Figure 4), an ejected electron has to be removed to quite some distance from the molecular layer until it reaches the nominal E^{∞}_{vac}. Furthermore, it has to overcome a potential barrier in the form of the extended region of higher electrostatic potential above the π-electron clouds next to the layer.[71] Consequently, the energy denoted as IE' in Figure 5a is actually required to remove an electron from the 2D molecular assembly. In the present case of lying unsubstituted molecules, $E_{vac} > E^{\infty}_{vac}$, and therefore $IE' > IE$. Similar rationale holds for *EA*.

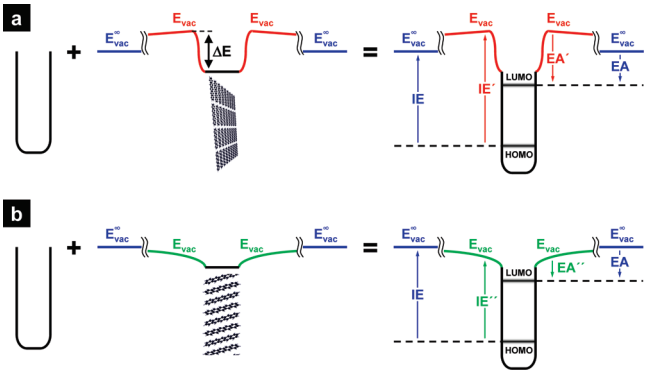

Figure 5. (a) Potential well caused by the nuclei and the core- and σ-electrons in a layer of lying π-conjugated or aromatic planar molecules is centered on the molecular plane (left panel). The π-electron clouds on both sides of the layer created an additional potential trough (center panel) of depth ΔE. These two together yield the total potential well felt by the electrons in the layer (right panel). Also indicated is the local vacuum level just outside the finite-size layer, E_{vac}, the vacuum level infinitely far away from the layer, E^{∞}_{vac}, and the corresponding ionization energies and electron affinities, IE' and EA' and *IE* and *EA*, respectively. (b) Same for a layer of standing molecules. Here, E_{vac} directly outside the layer is smaller than E^{∞}_{vac}, leading to the corresponding IE'' and EA''.

Next, we carefully reexamine Figure 4c to realize that close to the hydrogen-terminated "ends" of an isolated unsubstituted molecule, a region of lower potential energy can be found (cf. Figure 1b) owing to the positive charge on the molecular plane and, to some extent, also to the polarity of the $H^{\delta+}-C^{\delta-}$ bonds. Consequently, in a close-packed layer of standing unsubstituted molecules, this region of lower E_{vac} extends farther into space from the surface and lateral inhomogeneities in the potential again decay on the length scale of intermolecular distances;[52] this situation is sketched in Figure 5b. In contrast to the case of lying molecules, E_{vac} directly above a standing layer is now lower than E^{∞}_{vac} and, introducing the energy difference between this specific E_{vac} and the HOMO and LUMO as IE'' and EA'', respectively, one finds that $IE'' < IE$ and $EA'' < EA$.

The rigorous definition of *IE* and *EA* of course still holds, even if it technically means promoting an electron out of the layer to infinity (*IE*) or bringing an electron into the layer from infinity (*EA*). Nevertheless, the question arises, which of the *IE*s and *EA*s shown in Figure 5 are the electronic material parameters that actually determine the energy-level alignment between the molecular thin film and other (in)organic materials in a functional device. To address this question, the two cases of a metallic substrate in contact with layers of either lying or standing molecules are contrasted in Figure 6. To not unnecessarily complicate the discussion, the potential impact of metal/organic interface effects is commented

on at the end of this section. Here, the electrostatic potential energy is assumed to reach the value E^{∞}_{vac} immediately outside the metallic substrate, and no further modification upon monolayer adsorption is regarded.

For a layer of lying molecules, the situation prior to contact with such a substrate, that is, at a large distance, is schematically depicted in the left panel of Figure 6a. As established above, the electron potential energy (E_{vac}) is higher directly outside the π-systems that terminate both surfaces of the molecular layer than far away from the (finite-sized) layer and directly above the substrate (E^{∞}_{vac}).[34,71] As introduced in Figure 5a, the energy differences between the HOMO of the layer to E_{vac} and E^{∞}_{vac} are IE and IE', respectively. In the simplified scenario considered here (*vide supra*), the work function, Φ, of the substrate is the difference between its Fermi level, E_F, and E^{∞}_{vac}. Prior to contact, the HOMO thus lies at an energy $\Delta_h = IE - \Phi$ below E_F.

Without further interfacial phenomena (*vide infra*), the local vacuum levels directly outside the substrate and the molecular layer, E^{∞}_{vac} and E_{vac}, line up on contact (right panel in Figure 6a)—a situation commonly referred to as *vacuum-level alignment*.[34] As $E_{vac} > E^{\infty}_{vac}$, the potential well of the lying molecules is thus shifted down in energy with respect to E_F, that is, Δ_h increases to $\Delta'_h = IE' - \Phi$. Importantly, while the energy difference between an electron in the HOMO and an electron infinitely far away from the entire system is still IE, it is clearly IE' that defines the alignment of the HOMO with E_F; analogous considerations hold for EA' and LUMO alignment. Note that subsequent deposition of further layers (of lying molecules) amounts to simply adding further symmetric potential wells from the right with their local vacuum levels, E_{vac}, all aligned, which does not change the interface energetics.

The left panel of Figure 6b shows the situation for a (finite-sized) layer of standing molecules prior to contact with a metallic substrate, that is, when the two components are still separated by a large distance. As established in Figure 5b, there is an extended spatial region of slightly lower electron potential energy directly above the hydrogen-terminated surface of the molecular layer and the energy difference between the HOMO and this E_{vac} is IE''. Upon contact, the vacuum levels directly outside the two components, E_{vac} and E^{∞}_{vac}, again line up,[34] leading to the potential well of the standing layer being shifted slightly up in energy with respect to E_F, which results in a decrease of Δ_h to $\Delta''_h = IE'' - \Phi$. Again, the energy levels of substrate and molecular layer align as if the latter were characterized by the double-primed quantities (Figure 5b), IE'' in the case of the HOMO. Deposition of further layers of standing molecules amounts to adding further symmetric potential wells from the right with their local vacuum levels, E_{vac}, all aligned, and therefore, the interface energetics remain unchanged.

The two cases summarized in Figure 6a,b underline that, for all practical purposes, a layer of lying conjugated molecules (or polymers) has a higher effective IE and EA, namely, IE' and EA', than a layer of *the same molecules* oriented with their planes perpendicular to the layer

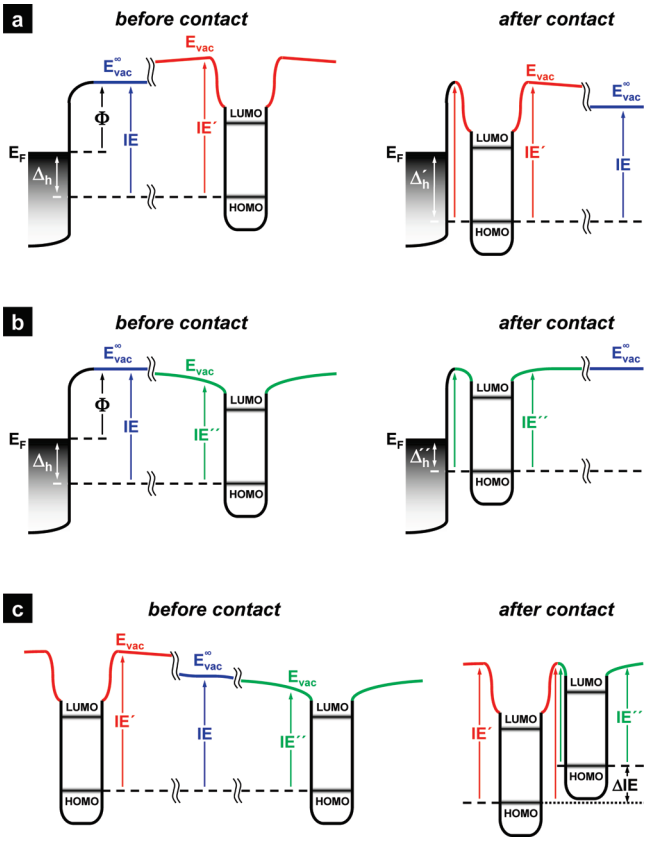

Figure 6. (a) Energy-level alignment between a finite-size layer of lying π-conjugated or aromatic planar molecules and a metallic surface when well separated (left panel) and after contact (right panel). The Fermi level, E_F, and the work function, Φ, of the metal are indicated as well as the vacuum level outside metallic substrate, E^{∞}_{vac}, and directly next to the molecular layer, E_{vac}. With respect to these reference energies, the molecules exhibit a ionization energy of IE and IE', respectively. Also marked are Δ_h and Δ'_h as the energy differences between E_F and the highest occupied molecular orbital (HOMO) in both cases. (b) Same for a layer of standing molecules, where E_{vac} directly outside the layer defines the ionization energy IE'' and Δ''_h, the energy difference between the HOMO and E_F after contact. (c) Energy-level alignment between a layer of lying (left) and a layer of standing (right) molecules at large separation (left panel) and after contact (right panel), where an energy offset of ΔIE between the respective HOMOs is observed.

surface, where IE'' and EA'' are the relevant quantities. To further highlight the important consequences of these findings, the interesting scenario can be constructed where a layer of lying molecules is brought into contact with a layer composed of identical molecular species oriented in a standing manner. The energy-level diagram for large separation of the two molecular layers is sketched in the left panel of Figure 6c. The common vacuum levels (E^{∞}_{vac}) far from the individual layers align. With respect to this reference energy, both layers have, of course, the same ionization energy and electron affinity, IE and EA. Locally, however, the vacuum level E_{vac} is higher than E^{∞}_{vac} directly outside the lying layer and lower just outside the standing layer, thus defining IE' and IE'' as introduced above (Figure 5). When the two molecular layers are brought into contact (i.e., to within a few angstroms) and no additional interfacial phenomena occur, the local vacuum levels above each surface align (right panel in Figure 6c). Consequently, the potential

well and the MOs of the lying layer are shifted down in energy with respect to those of the standing layer which, intriguingly, leads to an energy offset, ΔIE, between the HOMO levels in the two layers. Reminiscent of reports on inorganic semiconductors,[72,73] an electronic *hetero*junction is formed with two layers of the *same* molecular species, that is, at a material *homo*junction. Also in this case, it is clearly the energy differences between the frontier MOs and E_{vac} directly outside the respective layer, $IE'^{(\prime)}$ and $EA'^{(\prime)}$, that are the relevant electronic material parameters for interfacial energy-level alignment and *not* the nominal *IE* and *EA* values with respect to E^{∞}_{vac}.

To summarize this subsection, the positions of the frontier energy levels in a thin film of preferentially oriented molecules relative to E^{∞}_{vac}, the vacuum level infinitely far from the system, might be the rigorous definition of *IE* and *EA*, but they are irrelevant in practice. What does matter is the *relative* position of the energy levels in two materials *when these materials are in intimate contact*. Hence, for all practical purposes where molecular thin films are integrated into functional devices and are, therefore, in contact with (in)organic electrodes or other materials, E_{vac} directly above the surface that terminates the organic layer is the relevant reference energy and not E^{∞}_{vac}. Consequently, it is $IE'^{(\prime)}$ and $EA'^{(\prime)}$ that characterize the relevant energy levels of organic semiconductors.

3.4. Metal/Organic Interface Effects. It is important to realize that the π-system dipole layer is an intrinsic *surface* property of organic semiconductors and that, therefore, the phenomena just described are entirely decoupled from metal/organic or organic/organic *interface* effects.[34−39] Depending on the specific situation encountered in experiment (e.g., the metallic material or surface contamination),[37,74] such effects may or may not occur in real-world samples, but if they do, they are simply superimposed onto the orientational phenomena discussed in the last subsection, that is, they occur *in addition*.

For example, if the metallic electrode assumed above were an atomically clean metal surface in ultrahigh vacuum (UHV), adsorption of either standing or lying molecules would both reduce the metal surface dipole via the "push-back", "pillow", or "cushion" effect arising from Pauli repulsion between electrons in the molecules and the electron cloud spilling out into the vacuum from the metal surface.[75−78] Consequently, the entire molecular potential well together with the respective frontier orbitals would be rigidly shifted down in energy both in the standing and in the lying case. Naturally, such a shift would increase Δ'_h or Δ''_h as much as it would result in a decrease of the work function of the entire system. Importantly, however, the ionization energy (electron affinity) of the organic layer, IE' (EA') or IE'' (EA''), remains completely unaffected by such an interface dipole which, more precisely, actually corresponds to a modification of a surface property of the metal in this context.

Likewise, should the HOMO or the LUMO of the organic layer too closely approach the substrate E_F, Fermi-level pinning[38,79−84] will surely occur. If, for instance, the HOMO of a lying layer were already close to E_F, then the HOMO of a layer where the same molecules are standing would come to lie above E_F, which is prevented by electron transfer from the organic layer to the metal; the resulting dipole layer shifts the entire potential well of the molecular layer down in energy to ensure a minimum Δ''_h, thus reducing the work function of the entire system but, again, leaving the IE'' and EA'' of the standing layer itself unaltered.[85]

Finally, should electronic interactions of the organic with either the metal or other organic layers give rise to a continuous density of states at the respective interface,[86−94] then the equilibration of the electron chemical potential across the entire system might lead to additional interface dipoles, again leaving the $IE'^{(\prime)}$ and $EA'^{(\prime)}$ values intact. Further effects, for example, the stabilization of the ionization and affinity levels through screening by the metal surface,[95−98] superimpose on the orientational phenomena resulting from intrinsic molecular surface dipoles as well.

4. Experimental Evidence

4.1. Notes on Experimental Methods. Prior to reviewing experimental results that provide evidence for all three cases shown in Figure 6, experimental techniques that are commonly employed to derive interfacial energy-level alignment need to be critically assessed. Importantly, the preceding discussion allows the conclusion that any experimental method that operates on isolated molecules, for example, in gas phase or in solution, cannot yield the ionization energies and/or electron affinities relevant for the relative level alignment between organic thin films of preferentially ordered molecules and other materials. As outlined above, the reason is that the electron potential energy around an isolated molecule decays to a common vacuum level $E_{vac} = E^{\infty}_{vac}$ within a few angstroms (Figure 4) and, therefore, only one single *IE* and one *EA* can be determined with respect to this reference energy. Even taking into account other solid-state effects (e.g., electrostatic screening of an extra charge on a molecule via polarization of its environment),[98−106] numbers obtained by such experiments might only serve as estimates for the *IE* and *EA* values of amorphous molecular layers. In general, however, thusly determined *IE*s and *EA*s must be expected to differ appreciably from the actual ionization and affinity levels of a layer of preferentially oriented molecules. In particular, layers of lying or standing molecules exhibit the well-defined but distinctly different values of IE' and EA' or IE'' and EA'', respectively, neither of which equal *IE* and *EA*. Consequently, quantitatively and even qualitatively wrong interfacial energy-level alignment could be predicted from experiments on isolated molecules. Most drastically, from such measurements it is impossible to understand, let alone predict, the situation outlined in Figure 6c, that

is, the energy offset between the frontier MOs of two layers composed of identical molecules but with different orientations. The energy of the local vacuum level, E_{vac}, above the surface of a close-packed organic thin film of preferentially oriented molecules arises from a *collective* electrostatic effect, that is, the superposition of the potentials created by the π-system dipoles μ_π (Figure 4) of all molecules within the layer, or the absence thereof. Therefore, experiments must be performed on laterally extended layers. Only then can one aspire to deduce the energetic position of the ionization and affinity levels with respect to E_{vac}, which are the actually relevant parameters for the interfacial energy-level alignment between two materials.

For the occupied manifold of MOs, the HOMO in particular, ultraviolet photoelectron spectroscopy (UPS) is the method of choice,[107] as the measurement directly yields the energy required to remove an electron from a sample. Importantly, via the position of the secondary electron cutoff, this technique also permits directly extracting the local vacuum level, E_{vac}, just above the sample surface, which is precisely the reference energy that determines the sought-after ionization energy.[71]

4.2. Orientation-Dependent Ionization Energies of Ordered Molecular Layers. After extensive conceptual considerations, the stage is now set to review and interpret actual experimental results on real-world samples. Starting with pentacene (PEN), one of the most prominent representatives for organic semiconductors, UPS data are shown for both the lying and the standing cases in Figure 7a (see inset for chemical structure). The origin of the energy scale is the respective vacuum level, E_{vac}, directly above the sample, and therefore, the binding energy directly translates into ionization energy. When sublimed onto atomically flat and clean metal surfaces in UHV, the (111) surface of a gold single crystal in this instance, PEN—like most π-conjugated or aromatic planar molecules—lies down flat in the first monolayer.[108−115] The corresponding UPS spectrum (labeled "lying") shows a distinct peak which corresponds to the molecular HOMO; the Fermi edge of the substrate, indicated as E_F, is still visible through the first monolayer. Following the convention in ref [107], the low binding-energy onset of the HOMO is chosen to determine the ionization energy of $IE' = 5.35$ eV.[116,117] In contrast, on silicon oxide, most rod-like organic semiconductors are found to grow "standing upright", that is, with their long molecular axis close to perpendicular to the surface. PEN is no exception in this regard,[32,118−122] and the corresponding UPS spectrum (labeled "standing") yields a significantly lower IE'' of 4.80 eV.[65,117,120] The substantial IE difference of $\Delta IE = 0.55$ eV between lying and standing orientations clearly demonstrates the collective effect of the intramolecular surface dipoles arising from the π-electron systems (see Figures 4−6).

A particularly intriguing case is shown in Figure 7b for the organic semiconductor α,ω-dihexylsexithiophene or DH6T (see inset for chemical structure). Sublimed onto atomically clean Ag(111) surfaces in UHV, this molecule

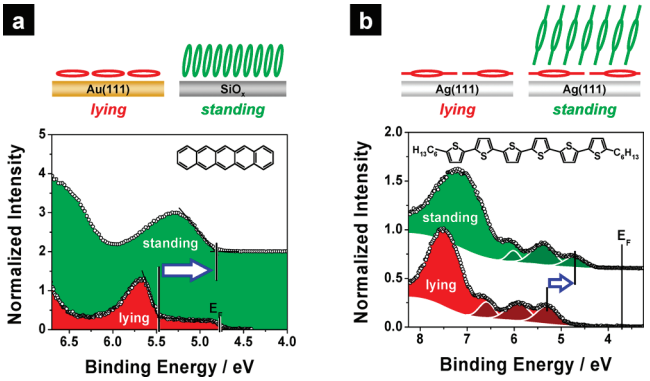

Figure 7. (a) Experimental UPS spectra of a lying monolayer of pentacene on the (111) surface of a gold single crystal (red)[116] and a thin film of standing pentacene on silicon oxide (green).[117] (b) The experimental UPS spectrum of a lying monolayer of α,ω-dihexylsexithiophene on Ag(111) is shown in red and that of the standing multilayer in green.[124] The energy reference is the vacuum level directly above the sample in each case and, for the metal substrates, the position of the Fermi level is indicated by E_F.

was shown to grow flat-lying in the first monolayer, whereas the second and all subsequent layers grow standing (almost) upright.[85,123−125] This peculiar growth mode allows demonstrating all three situations shown in Figure 6 on a single sample. The UPS spectrum of the first (lying) monolayer is shown in the bottom trace; the first three peaks are assigned to the HOMO, the HOMO-1, and the HOMO-2 in order of increasing binding energy (from right to left). Adhering to the convention chosen in the original publication,[124] $IE' = 5.3$ eV is taken as the binding energy of the HOMO *peak* (not the onset) with respect to E_{vac}. Upon deposition of more material onto the same sample, the UPS signature associated with layers of standing molecules gradually appears.[123] The final spectrum shown in the upper trace is rigidly shifted to lower binding energy, yielding a substantially lower IE'' of 4.7 eV.[124] Consequently, at the interface between the first lying layer and the second standing layer, an *electronic heterojunction* with a sizable energy-level offset of $\Delta IE = 0.6$ eV is formed between two layers of the *same* molecular species (DH6T), as predicted in Figure 6c. In contrast to the case of pentacene, where layers of standing molecules were measured on insulating silicon oxide, the well-defined Fermi level of silver in the case of DH6T permits extracting $\Delta'_h = 1.6$ eV and $\Delta''_h = 1.0$ eV (see also Figure 6),[124] the importance of which will be discussed in section 7. Notably, the sulfur *2p* core levels were seen to exhibit the same shift toward lower binding energies,[124] thus confirming that indeed *all* electrons in the molecular adlayers experience the same purely electrostatic effect of the intrinsic molecular surface dipole layer collectively formed by the π-electron systems.

Note that the data presented here do by no means reflect isolated occurrences. Numerous observations of orientation-dependent *IE*s can be found in literature for a variety of molecules on a wide range of substrates. Other examples include α-sexithiophene (6T),[124,126−128] *para*-sexiphenyl (6P),[67] perylene,[129] or copper(II) phthalocyanine (CuPc),[130−133] where ΔIE amounts to 0.4−0.8 eV, 0.3−0.6 eV, 0.3 eV, and 0.4 eV, respectively.

5. Surface Engineering with Intramolecular Polar Bonds

The data presented above unambiguously illustrate that the preferential orientation of molecules in an organic thin film appreciably impacts its ionization and affinity levels and, furthermore, also the relative alignment of these levels at organic/organic and organic/inorganic interfaces. These findings might suggest that controlling the molecular orientation provides a means to deliberately adjust interfacial energy-level alignments. In practice, however, not all orientations can readily be realized on all substrates, as the interrelation between film deposition methods/conditions and resulting molecular orientation is not always straightforward. More importantly, even if arbitrary orientations could be deliberately chosen for a given molecule/substrate combination, other constraints often make some molecular orientations preferable over others and what is gained by optimizing the interfacial energy-level alignment might be counteracted by concomitant detrimental factors. For instance, the inherently anisotropic (opto)electronic properties of most conjugated molecules often lead to equally anisotropic materials properties in ordered organic solids such as, for example, optical transition dipole moments or charge-carrier mobility. As the latter is typically higher in the direction perpendicular to the molecular planes (due to better intermolecular π-orbital overlap), it might be desirable to have this direction match that imposed by the external electrode geometry.

In the systems discussed so far, the orientation dependence of *IE* and *EA* was due to the presence or absence of the molecular π-electron system on the surface of an organic thin film. As the delocalized π-system is an integral feature of all organic semiconductors, this leaves little room for improvement through synthetic strategies. However, our considerations were restricted to unsubstituted molecules up to this point, where the surfaces in layers of preferentially standing molecules are terminated only by slightly positively charged hydrogen atoms. Notably, the rich chemistry of π-conjugated or aromatic molecules and polymers allows modifying these unsubstituted "ends" or "edges" by substitution with functional groups that either carry an intrinsic dipole moment themselves or withdraw/inject electrons from/into the π-system on the molecular core. This strategy opens up the possibility for electronic-structure engineering of organic semiconductors by means of surface modification with *intramolecular polar bonds* (IPBs).[117,120,134]

5.1. Back to Electrostatics. To consistently develop the strategy just introduced, it is insightful to first discuss a modified version of benzene (cf. Figure 4) in light of the electrostatic principles summarized in section 2. Specifically, two opposing hydrogen atoms are now substituted with fluorine, thus converting benzene into 1,4-difluorobenzene. The highly electronegative fluorine atoms draw electrons from the phenyl unit and, consequently, carry a negative partial charge, which is compensated by a positive partial charge in the benzene ring, as indicated in Figure 8a. Electrostatically, the situation is again strikingly similar to that depicted in Figure 1b, where a quadrupolar arrangement of point charges in a line is

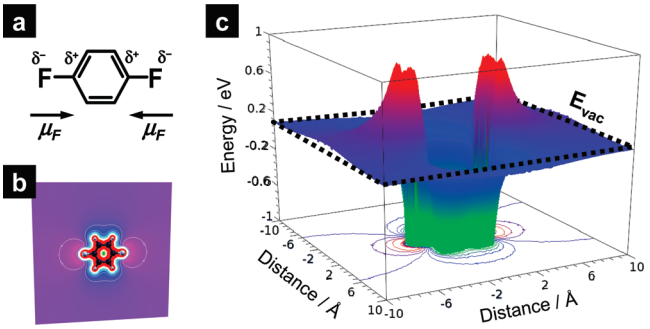

Figure 8. (a) Chemical structure of 1,4-difluorobenzene indicating the partial atomic charges and the related dipole moments, μ_F. (b) Plane through the molecule chosen for (c), where the electrostatic potential energy for electrons, as calculated by density-functional theory, is shown; a common vacuum level, E_{vac}, is established close to the isolated molecule.

realized by two dipoles pointing toward each other. Here, these dipoles, μ_F, arise from the polar $F^{\delta-}-C^{\delta+}$ bonds and, in contrast to benzene (Figure 4), they now lie *within* the plane of the molecule (Figure 8b), that is, its quadrupole moment is of different directionality. The 3D plot of the DFT-calculated electron potential energy in the molecular plane (Figure 8c) is almost indistinguishable from Figure 4c, where the same quantity is plotted for a plane perpendicular to that of the unsubstituted benzene molecule. In contrast, however, regions of higher potential energy are now found next to the fluorine atoms, and regions of lower potential are observed next to the remaining hydrogens in *ortho* and *meta* positions. Around the molecule, a common $E_{vac} = E_{vac}^{\infty}$ is rapidly established, which defines the ionization energy and the electron affinity, IE_F and EA_F, respectively, of an isolated 1,4-difluorobenzene molecule.

At this point, we emphasize that (a) the dipoles caused by the π-system are, of course, still present but are superseded by the stronger μ_F because the fluorine is now the "most negative" part of the system and, thus, determines the directionality of the molecular quadrupole moment;[135] (b) that fluorine—and also the subscript "F"—is to be understood as a placeholder for all moieties containing or causing intramolecular polar bonds; and (c) that such moieties need not directly interact with the π-electron system on the molecular core (*vide infra*).

Following the line of argument outlined in section 3, it is now easy to proceed from the isolated molecule to layers of preferentially oriented molecules. Clearly, the situation is now reversed compared to the case of unsubstituted molecules. While there, the surface of *lying* molecules is terminated by a layer of dipoles pointing toward the inside, that is, with the negative end on the outside, it is now the surface of *standing* molecules that is terminated by (more) negative fluorine atoms that give rise to a similar dipole layer. Consequently, the reverse scenario is to be expected for the ionization energy and the electron affinity of the end-fluorinated molecular layer, that is, the values of the standing layer, IE''_F and EA''_F, should now be higher than those of the lying layer, IE'_F and EA'_F.

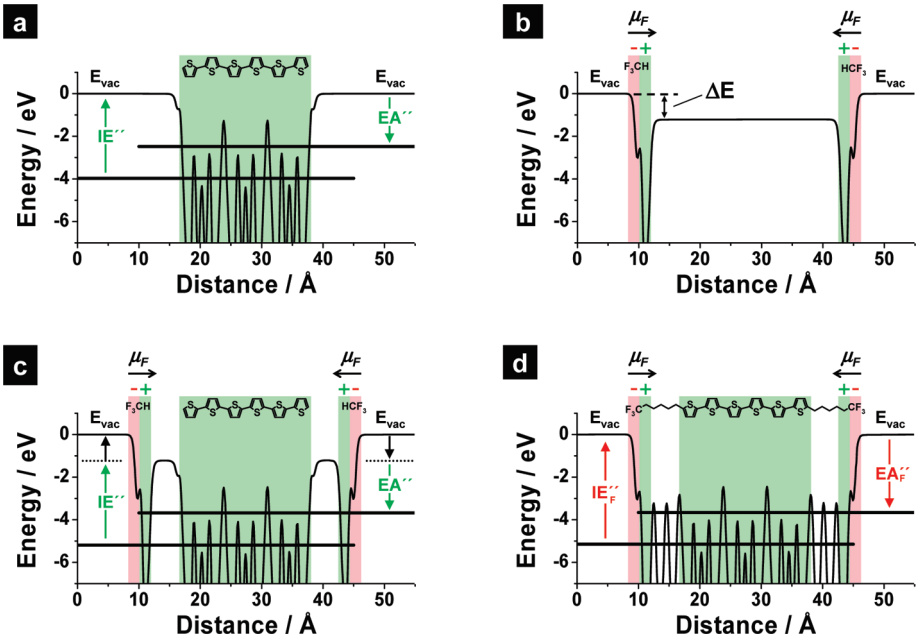

Figure 9. (a) Potential well of a layer of standing α-sexithiophene molecules (inset) as calculated by density-functional theory; the horizontal lines indicate the calculated HOMO and LUMO levels which, together with the vacuum level outside the layer, E_{vac}, define its ionization energy, IE', and its electron affinity, EA'. (b) Calculated potential well of depth ΔE created by two layers of CHF_3 with their strongly polar $F^{\delta-}-C^{\delta+}$ bonds (dipole moment μ_F) pointing toward the outside. (c) Calculated potential well of the standing α-sexithiophene layer from (a) placed between the two CHF_3 layers from (b). Chemically linking the molecular core to the $-CF_3$ groups by a *n*-pentane chain yields a new molecule (inset) with the calculated potential well shown in (d) and dramatically increased IE''_F and EA''_F.

5.2. Molecular Design. Both the validity of the concept and the strength of the approach are best illustrated with a computational experiment. Starting from an unsubstituted molecule, the DFT-calculated potential well across a 2D-infinite monolayer of standing 6T molecules (see inset) is shown in Figure 9a; the structure and the theoretical methodology are identical to those used in ref [124]. Also indicated are the calculated HOMO and LUMO levels (horizontal lines), the vacuum level (E_{vac}), and the associated IE'' and EA''.

According to Figure 3c, the spatial region between two dipole layers with their dipole moments pointing toward each other, that is, their negative ends on the outside, lies at a potential energy lower than the vacuum level outside the structure. One way of chemically realizing such opposing dipolar slabs is two layers of CHF_3 molecules (trifluoromethane) with the strongly polar $F^{\delta-}-C^{\delta+}$ bonds pointing toward the outside. Indeed, the DFT-calculated potential well of such a structure (Figure 9b) exhibits the expected characteristics, and in the present case, its depth amounts to $\Delta E = 1.2$ eV. Placing the layer of standing 6T molecules between the two dipolar CHF_3 layers lowers its entire potential well (together with the HOMO and LUMO levels) in energy relative to E_{vac} outside the dipole layers by ΔE. The results of the DFT calculation on this structure show that, to reach the vacuum level, an electron that is to be removed from the HOMO of the 6T layer now has to overcome an additional potential barrier of magnitude ΔE created by the CHF_3 dipole layer on either side (Figure 9c). Consequently, the ionization energy and electron affinity of the structure, $IE'' + \Delta E$ and $EA'' + \Delta E$, respectively, are now 1.2 eV higher than those found for the layer of standing 6T molecules alone (Figure 9a). To resolve this hypothetic structure into one entirely chemically plausible, the π-conjugated 6T core is now covalently linked to the terminal CHF_3 molecules by a linear *n*-pentane chain on both sides, that is, by a series of five nonconjugated methylene ($-CH_2-$) spacer units (see inset of Figure 9d for chemical structure). As the surface dipole moments are strictly located on the terminal $-CF_3$ units and, furthermore, the electronic structure of 6T is virtually unaffected by substituting the terminal hydrogen atoms with alkyl chains, the MO energies are essentially equal to those found in Figure 9c. The DFT-calculated ionization and affinity levels for a standing layer formed by the new end-fluorinated molecule, IE''_F and EA''_F, are exactly $\Delta E = 1.2$ eV higher than those of the original 6T layer.

Importantly, and this highlights the *collective* nature of the electrostatic effect of IPBs, the DFT-calculated IE and EA differences between unsubstituted 6T and the new fluorinated compound as *isolated* species in vacuum are <0.1 eV. Consequently, experimental methods that probe the electronic states of isolated molecules, such as cyclic voltammetry or gas-phase UPS, would find essentially no difference in the ionization and affinity levels of the two molecules, that is, they would find $IE \approx IE_F$ and $EA \approx EA_F$, and could not, therefore, explain their potentially different behavior in organic electronic devices. In contrast, UPS measurements on thin films of standing molecules are well capable of capturing the substantial difference between IE'' and IE''_F. These surprising findings also underline that the observed effect is of purely physical and not of chemical nature. The responsible dipolar $-CF_3$ groups are electronically completely decoupled from the π-electron system on the 6T core

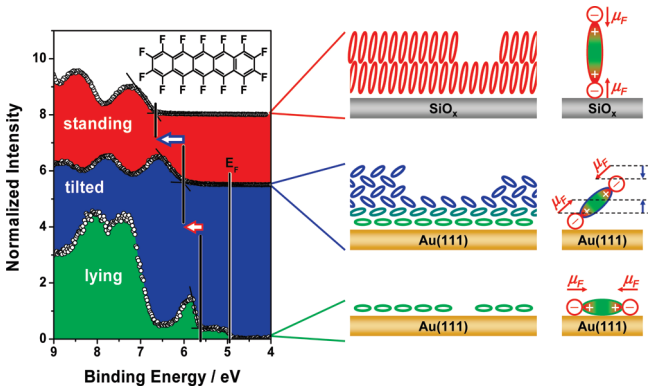

Figure 10. Experimental UPS spectra of perfluoropentacene (inset). That of a lying monolayer on Au(111) is shown in green,[116] that of inclined molecules in the multilayer is shown in blue,[116] and that of a film of standing molecules on silicon oxide is shown in red.[117] On the metal, the Fermi level is marked with E_F. The center panels indicate the molecular orientation in each case, and the right panels highlight the respective orientation of the dipole moment, μ_F, arising from the polar $F^{\delta-}-C^{\delta+}$ bonds relative to the surface and its projection onto the surface normal (blue arrows in middle panel).

(including the HOMO and LUMO localized there) by the insulating large band-gap alkyl segments. In other words, from the *physical* phenomenon of electric dipole layers, we have derived very concrete molecular design rules for *chemical* synthesis, thus underlining the benefit of an integrated multidisciplinary approach to organic electronics.

5.3. Experimental Evidence. The success of the strategy outlined above can be conveniently demonstrated on the example of the perfluorinated analogue to pentacene, perfluoropentacene (PFP). This choice permits directly contrasting PFP and PEN which are, in turn, closely related to the model compounds 1,4-difluorobenzene and benzene. PFP, like PEN, grows lying down flat in the first monolayer when deposited onto atomically clean metal surfaces under UHV conditions.[110,134,136,137] The bottom trace in Figure 10 shows the UPS spectrum of such a lying monolayer on the (111) face of a gold single crystal.[116] The Fermi edge of the substrate is clearly visible, and the first peak at $\Delta'_h = 0.85$ below E_F is the monolayer HOMO with its onset at a binding energy of $IE'_F = 5.80$ eV.[117] Upon further PFP deposition, a closed thicker film can be prepared as evidenced by the disappearance of the Fermi edge from the spectrum (center panel in Figure 10). Therein, the molecules are still lying with their long axes parallel to the substrate, but the molecular planes are inclined to the surface (center schematic in Figure 10). This is a consequence of the intermolecular interactions which, in the absence of molecule−substrate interactions in the multilayer, favor the typical "herringbone" packing motif found in the bulk crystal structure.[138−140] As the entire periphery is fluorine terminated in PFP, a surface dipole layer is formed by the projections of μ_F onto the surface normal, which point toward the substrate, that is, negative on the outside. Consequently, the HOMO is lowered with respect to both E_F and E_{vac}, and the ionization energy of the organic thin film increases to $IE_F^{\angle} = 6.00$ eV.[116] A similar behavior, both in terms of growth mode and electronic structure, has been observed for PFP on Ag(111) surfaces.[134] Like PEN, PFP also grows with its long molecular axis almost perpendicular to the layer surface on SiO$_x$ substrates.[120,141,142] A typical UPS spectrum of such a sample is shown in the topmost trace of Figure 10.[117,120] Since both the projection of μ_F onto the surface normal (top schematic in Figure 10) and the molecular packing density (eq 1) are higher in such a layer than in the case of the "tilted" molecules just discussed, the ionization energy further increases to $IE''_F = 6.65$ eV.[117]

As expected from the underlying electrostatics, the situation in PFP is reversed compared to PEN. There, films of standing molecules were found to have a *lower* ionization energy than films of lying molecules (by $\Delta IE = 0.55$ eV) due to the dipole layer formed by the π-electron clouds terminating the surface. In contrast, films of standing PFP have a *higher* ionization energy than films of lying molecules (by $\Delta IE_F = 0.85$ eV) owing to the close-packed IPBs on the surface, which lead to an additional potential step that an ejected electron has to overcome.

To appreciate the practical significance of the effect just demonstrated, let us consider that the ionization energies of isolated PEN and PFP molecules in gas phase, $IE = 6.6$ eV[143] and $IE_F = 7.5$ eV[144] differ by 0.9 eV; this to be expected as the fluorine substituents directly interact with the π-conjugated molecular core. Relying on this value, one would predict a HOMO offset of similar magnitude for an organic/organic interface between the two materials. In sharp contrast, the results presented above reveal that the HOMO offset in layered heterostructures of standing PEN and PFP molecules should be on the order of $IE''_F - IE'' = 6.65 - 4.80 = 1.85$ eV,[117] that is, more than twice the value (unjustifiably) deduced from measurements on isolated molecules. And indeed, UPS experiments on bilayer heterostructures confirm a HOMO offset of ~1.8 eV.[120] In the case of PFP, the *physical* effect of dipole-layer formation at the IPB-terminated surface of standing films (~0.9 eV) is of a magnitude comparable to the *chemical* effect (~0.9 eV) of direct interaction between fluorine substituents and the π-electron system.

Lastly, we remark that PFP is certainly not the only published example for the collective electrostatic action of IPBs. Similar observations have been made for perfluorinated copper(II) phthalocyanine (F_{16}CuPc), where the IE'_F of layers of lying molecules was seen to be *lower* by $\Delta IE_F = 0.85$ eV than the IE''_F of layers of standing (or rather "edge-on") molecules.[130−133] Recalling that the opposite was the case for the nonfluorinated analogue, CuPc, where the IE' of lying layers was *higher* by $\Delta IE = 0.4$ eV than the IE'' of standing layers,[130−133] the situation there is indeed comparable to that of PFP and PEN.

5.3.1. Mixed Materials. From the apparent similarities in the molecular and crystal structures of PFP and PEN, the question arises whether, via codeposition of PEN and PFP into mixed layers of standing molecules, the ionization energy of the composite materials can be continuously tuned between the limiting values of $IE'' = 4.80$ eV and $IE''_F = 6.65$ eV by varying the mixing ratio.[117] The magnitude of the potential energy step caused by the IPBs

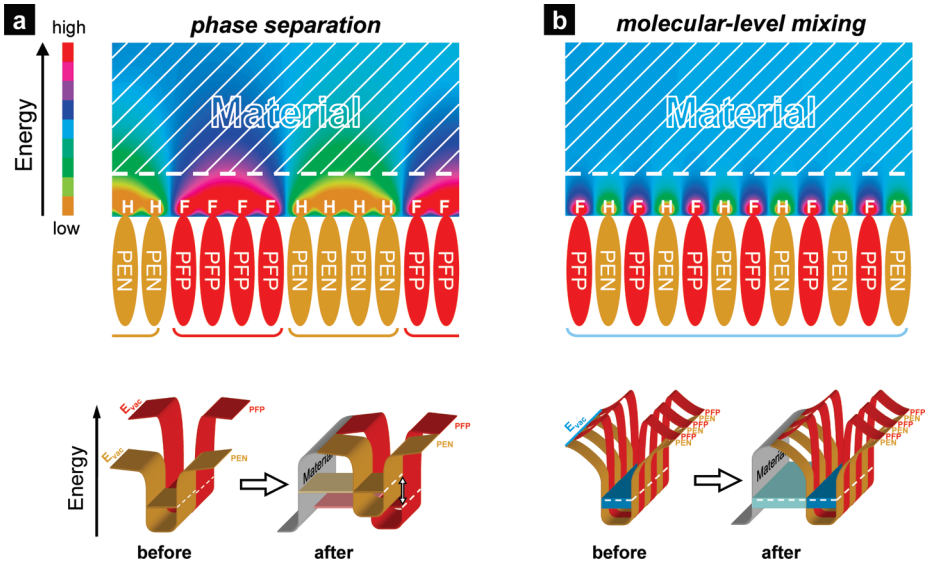

Figure 11. (a) Top panel shows a contour plot of the analytically calculated electron potential energy for a row of dipoles.[117] To represent macroscopic phase separation between pentacene (PEN) and pefluoropentacene (PFP), the row consists of alternating segments of four downward pointing dipoles (PFP) and four upward pointing dipoles (PEN). Clearly, a common vacuum level (E_{vac}) is *not* established within the distance to a different material in contact with the phase separated PEN/PFP layer. Consequently, PEN and PFP patches individually align the respective E_{vac} with that outside the material (bottom panel) leading to individual alignment of their frontier molecular orbitals (white dashed lines). (b) Scenario of molecular-level mixing. Top panel shows the electron potential energy for a row of alternating dipoles.[117] A common E_{vac} is established within the distance to a different material in contact with the mixed PEN/PFP layer. This common E_{vac} (bottom panel) aligns with that outside the material, leading to the laterally homogeneous alignment of the common electronic structure in the mixed layer.

exposed on the surface of such a mixed film must decrease as the dipoles are "diluted", that is, as the dipole area-density decreases (eq 1). To assess the feasibility of such an approach, we remember that it is the energy difference between the frontier electronic states in the mixed layer and the vacuum level *directly outside* the layer that must be varied in order to affect the energy-level alignment relative to other materials in close contact. Second, one has to bear in mind electrostatic principle (v) formulated in section 2, which says that inhomogeneities in the electrostatic potential outside a layer of discrete dipoles decrease on the length scale of the distance between the dipoles (Figure 2). Combining these two observations, one concludes that phase separation into large patches of standing PFP and standing PEN would be detrimental to the desired effect; E_{vac} would assume different values just outside either patch (top panel in Figure 11a) and, consequently, both PEN and PFP domains would *individually* align their respective energy levels with that of the substrate or of a subsequently deposited material (bottom panel in Figure 11a)—nothing would be gained, and instead of one organic semiconductor with intermediate ionization energy, two organic semiconductors (PEN and PFP) with largely different energy levels would, in fact, be obtained.

However, if one were to achieve mixing of PEN and PFP on the molecular level, the inhomogeneities in the potential outside the layer would decay on the length scale of intermolecular distances and a common E_{vac} would already be established within a few angstroms (Figure 11b). In this case, another material brought into contact with such a molecularly mixed film (i.e., to within a few angstroms) would no longer "see" the lateral inhomogeneities caused by the dilute $F^{\delta-}-C^{\delta+}$ dipoles on the layer surface and could, therefore, be expected to align to that common vacuum level (Figure 11b). In a recent experimental study[117] it was confirmed that molecular mixing can indeed be achieved for PEN and PFP and the desired effect was demonstrated by UPS experiments; the ionization energy of mixed layers could be continuously tuned between the limiting values of $IE'' = 4.80$ eV and $IE''_F = 6.65$ eV. Mixing, for example, D6HT (Figure 7b) with its end-fluorinated analogue (Figure 9d) or similar species allowing for mixed-crystal growth[145,146] could be expected to work equally well, thus outlining another nonsynthetic approach to tuning the relevant energy levels of organic semiconductors.

6. Intrinsic Surface Dipoles in Polymers

Throughout this Review, strong emphasis has been put on small-molecule organic semiconductors, so far largely neglecting the equally important class of conjugated polymers. Of course, the concepts described above hold for polymers as well. It is to be noted, however, that many polymers applied in organic electronic devices are essentially amorphous,[6,15−17,21−23,40,42,147,148] and therefore, orientational effects arising from the collective electrostatic action of the inhomogeneous charge distribution on individual chains or segments are not easily observed in macroscopic thin-film properties. However, if a preferential orientation of the polymer backbones can be achieved throughout the sample, the situation is again analogous to that encountered in the small-molecule case.

Maybe the most prominent example for a polymer where both a high degree of order and different orientations of the

polymer chains can be realized is head-to-tail regioregular poly(3-hexylthiophene); the chemical structure of this polymer (P3HT) is shown in the upper left panel of Figure 12. Its planar backbone together with the hexyl side chains promote self-organization among the polymer chains,[149] and highly ordered domains (embedded in an amorphous matrix) are frequently observed.[150−160] The degree of crystallinity and the morphology of P3HT films critically depend on the preparation conditions,[29,156−167] its molecular weight,[156,166−171] and the degree of regioregularity.[160,170] Samples with a preferentially "face-on" orientation (equivalent to a lying orientation in the small-molecule case) and films with a preferentially "edge-on" orientation of the polymer backbones in the crystalline domains can be reproducibly fabricated.[155−157] However, the orientation of the polymer backbones in the very surface layer of a P3HT film, that is, that in contact with the substrate or other materials, is still not easily accessible in experiment due to inevitable bulk contributions in the measurements.[172−177]

Circumventing these technical issues, both the occurrence and the importance of surface dipole layers in P3HT have recently been reported in a purely theoretical study.[135] There, as a model for the surface polymer layer of an ordered domain, a monolayer of P3HT has been considered. Different orientations of the polymer chains were realized by continuously increasing the angle, θ, between the polymer backbone and the plane of the layer (see inset in Figure 12) from the face-on configuration at $\theta = 0°$ to the edge-on configuration at $\theta = 90°$. The results of extensive DFT calculations on these structures are summarized in Figure 12. For P3HT (green traces), a decrease of both the ionization energy and the electron affinity was observed with increasing θ. Similar to the small-molecule case, the difference between the IE' in the face-on configuration and the IE'' in the edge-on configuration was found to be $\Delta IE \approx 0.4$ eV and was attributed to the surface dipole layer arising from the π-electron system on the polymer backbones (compare Figure 4).[135] The theoretically obtained ΔIE compares well with the spread in experimentally observed IE values (4.3−4.9 eV),[177−182] suggesting different preferential orientations of the polymer chains to be the cause thereof. Notably, through electrostatic modeling, a numerical value for the surface dipole moment could be extracted from the DFT data, yielding $\mu_\pi \approx 1.1$ D per thiophene ring.

Provided sufficiently well ordered films can be made, also the concept of electronic-structure engineering via surface modification with IPBs is applicable to polymers. To demonstrate this, the polymer shown in the upper right panel of Figure 12 was proposed in the same theoretical study.[135] Similar to the compound in Figure 9d, the methyl units at the ends of the hexyl side chains are now fluorinated, thus giving rise to strongly polar $F^{\delta-}-C^{\delta+}$ bonds with their net dipole moment, μ_F, pointing toward the polymer backbone (i.e., negative on the outside). As anticipated (cf. Figure 10), the situation is now reversed compared to unsubstituted P3HT and, with increasing θ, a sizable *increase* of up to 1.8 eV is found for IE_F and EA_F. From an extended electrostatic model that includes the contributions of both μ_π and μ_F, a value of ~2.5 D per $-CF_3$ unit was found for the latter.[135] Notably, the ionization energies and electron affinities of the two polymers are identical for the face-on orientation ($\theta = 0°$), where the π-electron clouds on the backbones terminate the surface in both cases. This fact highlights that the observed orientation dependence is of purely physical origin (collective electrostatic action of μ_π and μ_F, respectively) and that direct chemical interaction of the $-CF_3$ groups with the π-system on the polymer core, for example, of electron withdrawing or inductive nature, need not be invoked.

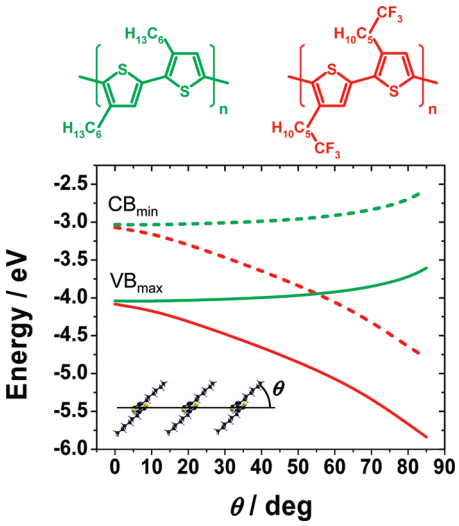

Figure 12. Calculated evolution of the valence-band maximum (VB_{max}) and the conduction-band minimum (CB_{min}) for polymer monolayers as a function of the angle, θ, between the planes of the polymer backbones and the plane of the layer (inset); values are reported relative to the vacuum level outside the respective layers. Chemical structures are shown in the upper panels.

7. Implications for Devices

In order to discuss organic (opto)electronic devices in the context of this Review, one has to distinguish between amorphous and ordered organic thin films, both for the small-molecule and the polymer case. In particular, amorphous organic layers are often found in OLEDs[5,13−17,40,41,147,148] and OPVCs.[21−23,42] There, it is important to consider whether the films are amorphous only macroscopically, that is, ordered domains exist but are oriented randomly throughout the sample, or whether the films are truly amorphous on the molecular scale, that is, not even short-range order exists in the sample. In the latter case, as with the mixed layers discussed in subsection 5.3.1, lateral inhomogeneities on the film surface (some molecules expose the π-system on the surface, others their edges or ends) decay on the length scale of intermolecular distances,[52] and a common vacuum level is established immediately above the layer surface. Consequently, if a microscopically amorphous thin film is brought into contact with another material, the interfacial energy-level alignment will be homogeneous over the entire interface. If, however, ordered domains (of a few nanometers or larger) of differently oriented molecules/polymers are present at the film surface, then the energy difference between the frontier electronic states and the *local*

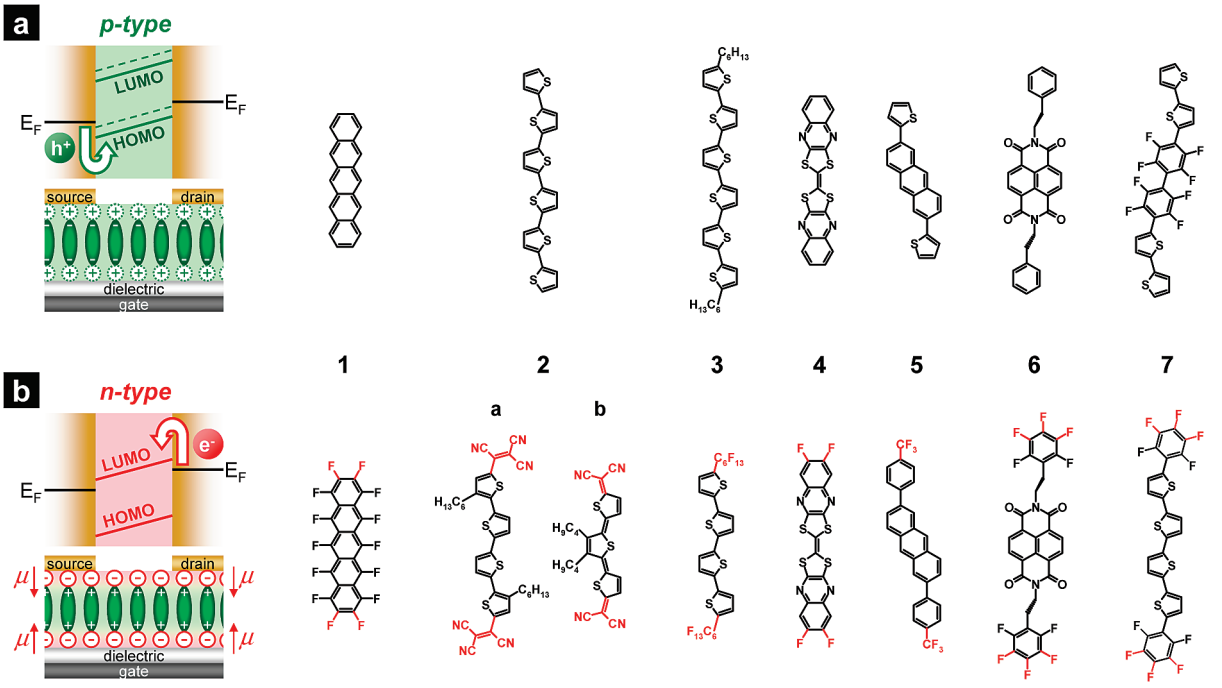

Figure 13. (a) Schematic of a *p*-type organic field-effect transistor (lower panel) with a film of standing molecules as active organic layer and the relevant energy levels under bias (upper panel); vertical lines indicate the source and drain Fermi levels, E_F, and solid slanted lines represent the HOMO and LUMO of the organic semiconductor. Terminating the "ends" of the organic molecules with dipolar groups (positive on the outside) shifts the bands up in energy (dashed slanted lines), thus further reducing the barrier for hole (h^+) injection. Compounds **1**−**7** are examples for typical *p*-type molecules. (b) Same as (a) for the *n*-type case. The surface dipole layer, μ, that arises from the electron-withdrawing groups at the ends of the *n*-type molecules **1**−**7** (highlighted in red) brings the LUMO down in energy with respect to E_F, thus lowering the barrier for electron (e^-) injection.

vacuum level just outside the respective domain will vary from domain to domain. Consequently, each patch will individually and differently align its energy levels with that of another material brought into close contact, and the level alignment will be inhomogeneous at the interface. For OLEDs this implies that, for example, the efficiency of charge-blocking or -injection layers might vary locally at an organic/organic interface or that the barriers for charge-carrier injection from external electrodes might vary locally. In principle, such effects might also contribute to the frequently observed local degradation of such devices.[183−188] For OPVCs, on the other hand, a locally different energy-level alignment at the interface(s) between donor and acceptor components might result in a locally varying efficiency for exciton dissociation and, thus, charge-carrier generation.

7.1. Organic Field-Effect Transistors. For OFETs, the need for high charge-carrier mobility requires good intermolecular π-orbital overlap over comparatively large distances, which makes a high degree of order, or even better crystallinity, desirable. Naturally, best performance is obtained when the direction of highest charge-carrier mobility coincides with the source-drain direction imposed by the device geometry. Indeed, in a planar setup, a preferentially edge-on orientation of P3HT on the gate dielectric was seen to be beneficial, while a preferentially face-on orientation was found to be detrimental for transistor performance.[155,157,158,162] In the small-molecule case, the prototypical rod-shaped species discussed repeatedly in this Review (i.e., PEN, 6T, and DH6T) are known to form (poly)crystalline layers of standing molecules on typical gate dielectrics (e.g., silicon oxide),[32,118,119,189] thus naturally aligning the direction of strongest π-orbital overlap and highest charge-carrier mobility in the desired way.

While these constraints on the molecular/polymer orientation preclude tuning of the energy levels via the dipole moments associated with the omnipresent π-systems, the standing/edge-on orientation opens up the possibility for adjusting the ionization and affinity levels via IPBs at the molecular ends or edges that are exposed at the surfaces of ordered thin films. In particular, we consider the *top-contact* device configuration here, where source and drain electrodes are deposited on top of the active organic layer, thus defining the channel region (see Figure 13). Commenting on the unsubstituted case first, it is to be noted that many molecules and polymers such as, for example, PEN, 6T, DH6T, or P3HT (see Figure 13a for more), work best as *p*-type organic semiconductors, that is, with a negative gate voltage applied in an OFET and holes as the primary charge carriers.[26−32,155,162−167,171,189−193] Recalling that no organic semiconductor is intrinsically *p*- or *n*-type and, in principle, both holes and electrons can be transported through the material,[194] this observation can be attributed to the energy-level alignment in the device.[195] As sketched in Figure 13a, the HOMO of so-called *p*-type materials is typically closer to the Fermi level of source and drain electrodes than the LUMO. Consequently, already a relatively small negative gate voltage can push the HOMO above E_F, leading to hole accumulation and, thus, to mobile charge carriers in the channel. Moreover, charge-injection from the source electrode into the

organic is enhanced if the energy difference Δ''_h between HOMO and E_F (the *hole-injection barrier*) is small.

With that in mind, we note that the standing/edge-on orientation is favorable not only because the direction of highest mobility coincides with the source-drain direction but also because the HOMO is further up in energy than in the lying/face-on case, thus further promoting lower threshold voltages and reducing hole-injection barriers.[124,135] As indicated in the bottom schematic in Figure 13a,[135] decorating the surface of such a standing/edge-on layer with IPBs that have their dipole moment pointing *away* from the surface (*positive* on the outside) would bring the HOMO even further up and, thus, must be expected to further enhance *p*-type transistor performance.

To reduce power consumption in organic electronic circuitry, it is desirable to not only rely on *p*-type transistors, but rather to use complementary (CMOS) logic.[139,196,197] This requires equally well performing *n*-type OFETs where, through applying a positive gate voltage, electrons are accumulated in the channel to act as primary charge carriers. While a number of organic molecules that exhibit reasonable performance as *p*-type materials have been identified to date, the quest for comparable *n*-type materials is still ongoing.[31,32,195,198] As becomes apparent in the schematics in Figure 13, the question of *p*- or *n*-type behavior is mostly one of interfacial energy-level alignment.[195] For the situation sketched in Figure 13a, a considerably higher positive threshold voltage would be required to pull the LUMO far enough down in energy to actually inject electrons from the drain electrode; and even then, these electrons would have to overcome a substantial injection barrier of $\Delta''_e = E_{LUMO} - E_F$. One strategy to improve the situation would be to synthesize molecules/polymers with a particularly electron-poor π-conjugated or aromatic core, that is, organic semiconductors with a particularly low-lying LUMO. However, this may come at the cost of concomitantly decreasing the environmental stability of such materials, potentially leading to rapid degradation under device operation in the presence of air and humidity.

Recently, a series of molecules has emerged that exhibit both good *n*-type transistor performance and reasonable environmental stability (see Figure 13b for some examples).[138−140,195,199−210] Notably, although different ideas and design strategies were pursued for every compound, they are all characterized by strongly electron-withdrawing groups at their ends (highlighted in red). Even more intriguing is the fact that their LUMO is often not substantially lower in energy than that of their *p*-type counterparts when determined for the *isolated* species; cyclic voltammetry or quantum chemistry shows that, frequently, it is only lower by a few tenths of an eV, especially when the end-group substituents do not strongly interact with the π-electron system.[204−209] While this, at least in part, can explain their environmental stability, it seems too small a difference to revert their behavior as transistor materials from *p*-type to *n*-type, that is, to alter the situation from $\Delta''_h \ll \Delta''_e$ to $\Delta''_e \ll \Delta''_h$.

In view of the fact that also good *n*-type molecules grow in a layered mode with their long molecular axes (almost) perpendicular to the surface of the gate dielectric,[138,195,199−210] the effect of surface termination with IPBs can finally give a satisfactory explanation for the observed transistor behavior and thus unify the overarching design principle for *n*-type materials. It has been shown in preceding sections of this Review that the *EA* difference between two isolated molecules can be significantly enhanced in thin films of standing molecules. Given the comparable optical gaps of PEN and PFP,[120] the *EA* difference between the two molecules can be estimated to increase from 0.8 to 1.7 eV and, in the computational experiment shown in Figure 9, the *EA* difference between 6T (Figure 9a) and the end-fluorinated DH6T (Figure 9d) is found to increase from 0.1 to 1.2 eV. So rather than in the single-molecule properties, the key to understanding the *n*-type behavior of the molecules shown in Figure 13b lies, once again, in the collective electrostatic action of the dipoles at their ends. In a close-packed layer, these form steps in the electron potential energy (Figure 2) at both surfaces of the active organic film. The ensuing potential well (Figure 3c) pulls the spatial region between these two surface dipole layers, that is, the entire molecular film, down in energy with respect to the outside. In particular, the LUMO is thus shifted down in energy with respect to the source and drain Fermi level, Δ''_e is reduced, the (positive) threshold voltage is lowered, and electron injection is facilitated (schematic in Figure 13b). Following this rationale, also the end-fluorinated P3HT (Figure 12) should be a good candidate for polymeric materials that exhibit enhanced *n*-type transistor action[135] provided that highly ordered films with a predominantly edge-on orientation can be realized and that additional factors detrimental to electron transport can be controlled.[32,194,195]

8. OUTLOOK

Whenever highly ordered organic semiconductors are employed, the molecular orientation with respect to a relevant interface, for example, the donor/acceptor interface in (discrete) heterojunction OPVCs or the organic/inorganic interfaces in OFETs, appreciably affects the energy-level alignment at that interface. If a standing/edge-on orientation is both desired and achievable at such an interface, then the insights reviewed here permit formulating some guidelines for molecular design. As the transport of both charges and optical excitations is mediated by intermolecular $\pi-\pi$ interactions, the conjugated or aromatic molecular core should be optimized with regard to maximizing intermolecular electronic coupling. As the latter critically depends on details in the molecular packing, developing a thorough understanding of the interrelation between molecular and crystal structure is both a much-needed requirement and a formidable challenge to the community.[45−49] Importantly, under the circumstances just mentioned, the introduction of intramolecular polar bonds somewhat alleviates the requirement of simultaneously having to keep the frontier molecular orbitals at their optimal energies for a given application. Once a desirable solid-state packing is achieved, grafting polar side groups onto the molecular ends or edges that are exposed at the relevant interface permits shifting the energy levels of the molecular layer

with respect to other materials in close contact. With the dipole moment of such a group pointing toward the molecular layer in question its MOs are shifted down in energy, and conversely, with the dipole moment pointing away from the molecular layer its MOs are shifted upward. Furthermore, it might be desirable not to directly attach such dipolar side groups to the molecular core, but to tether them with an alkyl spacer, as this might (a) promote layered growth of the molecules through "phase separation" of π-conjugated/aromatic core and alkyl segments,[145,146,189,209−211] (b) prevent unwanted changes to the electronic structure of the molecular core, and (c) open up the possibility for mixing species with different polar groups at the end of the alkyl side chains without perturbing the packing of the conjugated molecular cores (see also subsection 5.3.1).

9. Summary and Conclusions

To summarize, the surface termination of layers comprising preferentially oriented molecules or polymers critically impacts their effective ionization energies and electron affinities and, consequently, the energy-level alignment at interfaces with other organic or inorganic materials. The π-electron systems of aromatic or conjugated planar molecules and polymers collectively form a surface dipole layer in thin films of predominantly lying/face-on species, which is not present in thin films of predominantly standing/edge-on species. Deduced from fundamental electrostatic principles, the presence or absence of this intrinsic surface dipole layer leads to a pronounced dependence of the ionization energies and electron affinities of an organic thin film on the orientation of the constituent molecules or polymer chains with respect to its surface. Using ultraviolet photoelectron spectroscopy on thin-film samples as a reliable experimental tool to determine the energies of the occupied electronic states with respect to the relevant reference energy (i.e., the vacuum level directly outside the sample), experimental evidence for the expected orientational effect was provided.

For the case of preferentially standing or edge-on orientation of the molecules (or polymer chains) in organic thin films, substituting dipolar groups onto the exposed "ends" or "edges" of the aromatic or π-conjugated core was shown to equally lead to the formation of a surface dipole layer. Again, the presence or absence thereof was shown to appreciably impact the energies of the ionization and affinity levels in organic thin films, both through experimental evidence and extensive first-principles calculations. In analogy to the surface modification of inorganic electrodes to modify their work function,[212−220] intramolecular polar bonds were introduced as a means for the surface engineering of ordered organic semiconductors.

The importance of intrinsic molecular surface dipole layers on the energy-level alignment at ubiquitous organic/organic and organic/inorganic interfaces in organic (opto)electronic devices was discussed. Controlling the molecular orientation in the active organic layers of such devices was shown to be a necessary prerequisite and an important tool for tailoring the interfacial level alignment to application-specific demands. In particular, the collective electrostatic effect of intramolecular polar bonds was shown to not only improve but to even define device characteristics in organic field-effect transistors. From a thorough understanding of molecular-scale electrostatics, valuable guidelines for molecular and materials design could be derived, thus contributing to the continuous feedback loop that drives progress in the inherently multidisciplinary field of organic electronics.

Acknowledgment. This work was financially supported by the DFG. S.D. gratefully acknowledges a JSPS fellowship for foreign researchers.

References

(1) Forrest, S. R. *Nature* **2004**, *428*, 911–918.
(2) Sekitani, T.; Someya, T. *Adv. Mater.* **2010**, *22*, 2228–2246.
(3) Zschieschang, U.; Ante, F.; Yamamoto, T.; Takimiya, K.; Kuwabara, H.; Ikeda, M.; Sekitani, T.; Someya, T.; Kern, K.; Klauk, H. *Adv. Mater.* **2010**, *22*, 982–985.
(4) Katz, H. E. *Chem. Mater.* **2004**, *16*, 4748–4756.
(5) Pardo, D. A.; Jabbour, G. E.; Peyghambarian, N. *Adv. Mater.* **2000**, *12*, 1249–1252.
(6) Sirringhaus, H.; Kawase, T.; Friend, R. H.; Shimoda, T.; Inbasekaran, M.; Wu, W.; Woo, E. P. *Science* **2000**, *290*, 2123–2126.
(7) Stutzmann, N.; Friend, R. H.; Sirringhaus, H. *Science* **2003**, *299*, 1881–1884.
(8) Bao, Z. N.; Feng, Y.; Dodabalapur, A.; Raju, V. R.; Lovinger, A. J. *Chem. Mater.* **1997**, *9*, 1299–1301.
(9) Garnier, F.; Hajlaoui, R.; Yassar, A.; Srivastava, P. *Science* **1994**, *265*, 1684–1686.
(10) Kelley, T. W.; Baude, P. F.; Gerlach, C.; Ender, D. E.; Muyres, D.; Haase, M. A.; Vogel, D. E.; Theiss, S. D. *Chem. Mater.* **2004**, *16*, 4413–4422.
(11) Sekitani, T.; Yokota, T.; Zschieschang, U.; Klauk, H.; Bauer, S.; Takeuchi, K.; Takamiya, M.; Sakurai, T.; Someya, T. *Science* **2009**, *326*, 1516–1519.
(12) Klauk, H. *Chem. Soc. Rev.* **2010**, *39*, 2643–2666.
(13) Sun, Y. R.; Giebink, N. C.; Kanno, H.; Ma, B. W.; Thompson, M. E.; Forrest, S. R. *Nature* **2006**, *440*, 908–912.
(14) Gustafsson, G.; Cao, Y.; Treacy, G. M.; Klavetter, F.; Colaneri, N.; Heeger, A. J. *Nature* **1992**, *357*, 477–479.
(15) Cao, Y.; Parker, I. D.; Yu, G.; Zhang, C.; Heeger, A. J. *Nature* **1999**, *397*, 414–417.
(16) Burroughes, J. H.; Bradley, D. D. C.; Brown, A. R.; Marks, R. N.; Mackay, K.; Friend, R. H.; Burns, P. L.; Holmes, A. B. *Nature* **1990**, *347*, 539–541.
(17) Friend, R. H.; Gymer, R. W.; Holmes, A. B.; Burroughes, J. H.; Marks, R. N.; Taliani, C.; Bradley, D. D. C.; Dos Santos, D. A.; Bredas, J. L.; Logdlund, M.; Salaneck, W. R. *Nature* **1999**, *397*, 121–128.
(18) Tang, C. W.; VanSlyke, S. A. *Appl. Phys. Lett.* **1987**, *51*, 913–915.
(19) Sirringhaus, H.; Tessler, N.; Friend, R. H. *Science* **1998**, *280*, 1741–1744.
(20) Kim, J. Y.; Lee, K.; Coates, N. E.; Moses, D.; Nguyen, T. Q.; Dante, M.; Heeger, A. J. *Science* **2007**, *317*, 222–225.
(21) Sariciftci, N. S.; Smilowitz, L.; Heeger, A. J.; Wudl, F. *Science* **1992**, *258*, 1474–1476.
(22) Marks, R. N.; Halls, J. J. M.; Bradley, D. D. C.; Friend, R. H.; Holmes, A. B. *J. Phys.: Condens. Matter* **1994**, *6*, 1379–1394.
(23) Dennler, G.; Scharber, M. C.; Brabec, C. J. *Adv. Mater.* **2009**, *21*, 1323–1338.
(24) Tang, C. W. *Appl. Phys. Lett.* **1986**, *48*, 183–185.
(25) Peumans, P.; Uchida, S.; Forrest, S. R. *Nature* **2003**, *425*, 158–162.
(26) Horowitz, G.; Fichou, D.; Peng, X. Z.; Xu, Z. G.; Garnier, F. *Solid State Commun.* **1989**, *72*, 381–384.
(27) Paloheimo, J.; Kuivalainen, P.; Stubb, H.; Vuorimaa, E.; Ylilahti, P. *Appl. Phys. Lett.* **1990**, *56*, 1157–1159.
(28) Assadi, A.; Svensson, C.; Willander, M.; Inganas, O. *Appl. Phys. Lett.* **1988**, *53*, 195–197.
(29) Bao, Z.; Lovinger, A. J.; Dodabalapur, A. *Appl. Phys. Lett.* **1996**, *69*, 3066–3068.
(30) Dodabalapur, A.; Torsi, L.; Katz, H. E. *Science* **1995**, *268*, 270–271.
(31) Horowitz, G. *Adv. Mater.* **1998**, *10*, 365–377.
(32) Dimitrakopoulos, C. D.; Malenfant, P. R. L. *Adv. Mater.* **2002**, *14*, 99–117.
(33) Braga, D.; Horowitz, G. *Adv. Mater.* **2009**, *21*, 1473–1486.

(34) Ishii, H.; Sugiyama, K.; Ito, E.; Seki, K. *Adv. Mater.* **1999**, *11*, 605–625.
(35) Kahn, A.; Koch, N.; Gao, W. Y. *J. Polym. Sci., Part B* **2003**, *41*, 2529–2548.
(36) Koch, N. *J. Phys.: Condens. Matter* **2008**, *20*, 184008/1–12.
(37) Hwang, J.; Wan, A.; Kahn, A. *Mater. Sci. Eng., R* **2009**, *64*, 1–31.
(38) Braun, S.; Salaneck, W. R.; Fahlman, M. *Adv. Mater.* **2009**, *21*, 1450–1472.
(39) Koch, N. *Chem. Phys. Chem.* **2007**, *8*, 1438–1455.
(40) Bernius, M. T.; Inbasekaran, M.; O'Brien, J.; Wu, W. S. *Adv. Mater.* **2000**, *12*, 1737–1750.
(41) D'Andrade, B. W.; Forrest, S. R. *Adv. Mater.* **2004**, *16*, 1585–1595.
(42) Hoppe, H.; Sariciftci, N. S. *J. Mater. Res.* **2004**, *19*, 1924–1945.
(43) Peumans, P.; Yakimov, A.; Forrest, S. R. *J. Appl. Phys.* **2003**, *93*, 3693–3723.
(44) Rand, B. P.; Burk, D. P.; Forrest, S. R. *Phys. Rev. B* **2007**, *75*, 115327.
(45) Day, G. M.; Cooper, T. G.; Cruz-Cabeza, A. J.; Hejczyk, K. E.; Ammon, H. L.; Boerrigter, S. X. M.; Tan, J. S.; Della Valle, R. G.; Venuti, E.; Jose, J.; Gadre, S. R.; Desiraju, G. R.; Thakur, T. S.; van Eijck, B. P.; Facelli, J. C.; Bazterra, V. E.; Ferraro, M. B.; Hofmann, D. W. M.; Neumann, M. A.; Leusen, F. J. J.; Kendrick, J.; Price, S. L.; Misquitta, A. J.; Karamertzanis, P. G.; Welch, G. W. A.; Scheraga, H. A.; Arnautova, Y. A.; Schmidt, M. U.; van de Streek, J.; Wolf, A. K.; Schweizer, B. *Acta Crystallogr., Sect. B* **2009**, *65*, 107–125.
(46) Day, G. M.; Motherwell, W. D. S.; Ammon, H. L.; Boerrigter, S. X. M.; Della Valle, R. G.; Venuti, E.; Dzyabchenko, A.; Dunitz, J. D.; Schweizer, B.; van Eijck, B. P.; Erk, P.; Facelli, J. C.; Bazterra, V. E.; Ferraro, M. B.; Hofmann, D. W. M.; Leusen, F. J. J.; Liang, C.; Pantelides, C. C.; Karamertzanis, P. G.; Price, S. L.; Lewis, T. C.; Nowell, H.; Torrisi, A.; Scheraga, H. A.; Arnautova, Y. A.; Schmidt, M. U.; Verwer, P. *Acta Crystallogr., Sect. B* **2005**, *61*, 511–527.
(47) Desiraju, G. R. *Angew. Chem., Int. Ed.* **2007**, *46*, 8342–8356.
(48) Desiraju, G. R.; Gavezzotti, A. *Acta Crystallogr., Sect. B* **1989**, *45*, 473–482.
(49) Desiraju, G. R.; Gavezzotti, A. *J. Chem. Soc., Chem. Commun.* **1989**, 621–623.
(50) Forrest, S. R. *Chem. Rev.* **1997**, *97*, 1793–1896.
(51) Liu, S. H.; Wang, W. C. M.; Briseno, A. L.; Mannsfeld, S. C. E.; Bao, Z. N. *Adv. Mater.* **2009**, *21*, 1217–1232.
(52) Natan, A.; Kronik, L.; Haick, H.; Tung, R. T. *Adv. Mater.* **2007**, *19*, 4103–4117.
(53) Koopmans, T. *Physica* **1934**, *1*, 104–113.
(54) Koopmans' theorem is strictly valid only for unrelaxed excitations within the Hartree−Fock scheme, an approximate method by itself. More rigorously, ionization energy and electron affinity should be seen as the highest quasi-hole and lowest quasi-electron excitation energies (eigenvalues of the Dyson equation), respectively. Then, DFT eigenvalues can be reasonable approximations to these quantities under circumstances outlined in ref 55. Note that the DFT version of Koopmans' theorem, often referred to as Janak's theorem,[56] holds rigorously only for the ionization energy and then only if the exact exchange-correlation functional were known.[57, 58]
(55) Kümmel, S.; Kronik, L. *Rev. Mod. Phys.* **2008**, *80*, 3–60.
(56) Janak, J. F. *Phys. Rev. B* **1978**, *18*, 7165–7168.
(57) Perdew, J. P.; Parr, R. G.; Levy, M.; Balduz, J. L. *Phys. Rev. Lett.* **1982**, *49*, 1691–1694.
(58) Almbladh, C. O.; von Barth, U. *Phys. Rev. B* **1985**, *31*, 3231–3244.
(59) Dürr, A. C.; Koch, N.; Kelsch, M.; Rühm, A.; Ghijsen, J.; Johnson, R. L.; Pireaux, J. J.; Schwartz, J.; Schreiber, F.; Dosch, H.; Kahn, A. *Phys. Rev. B* **2003**, *68*, 115428/1–12.
(60) Resel, R. *Thin Solid Films* **2003**, *433*, 1–11.
(61) Ruiz, R.; Choudhary, D.; Nickel, B.; Toccoli, T.; Chang, K. C.; Mayer, A. C.; Clancy, P.; Blakely, J. M.; Headrick, R. L.; Iannotta, S.; Malliaras, G. G. *Chem. Mater.* **2004**, *16*, 4497–4508.
(62) Schreiber, F. *Phys. Status Solidi A* **2004**, *201*, 1037–1054.
(63) Zojer, E.; Koch, N.; Puschnig, P.; Meghdadi, F.; Niko, A.; Resel, R.; Ambrosch-Draxl, C.; Knupfer, M.; Fink, J.; Bredas, J. L.; Leising, G. *Phys. Rev. B* **2000**, *61*, 16538–16549.
(64) Witte, G.; Wöll, C. *J. Mater. Res.* **2004**, *19*, 1889–1916.
(65) Fukagawa, H.; Yamane, H.; Kataoka, T.; Kera, S.; Nakamura, M.; Kudo, K.; Ueno, N. *Phys. Rev. B* **2006**, *73*, 245310/1–5.
(66) Sato, N.; Seki, K.; Inokuchi, H.; Harada, Y. *Chem. Phys.* **1986**, *109*, 157–162.
(67) Ivanco, J.; Winter, B.; Netzer, T. R.; Ramsey, M. G. *Adv. Mater.* **2003**, *15*, 1812–1815.
(68) Winter, B.; Berkebile, S.; Ivanco, J.; Koller, G.; Netzer, F. P.; Ramsey, M. G. *Appl. Phys. Lett.* **2006**, *88*, 253111/1–3.
(69) Koller, G.; Berkebile, S.; Ivanco, J.; Netzer, F. P.; Ramsey, M. G. *Surf. Sci.* **2007**, *601*, 5683–5689.
(70) Yanagi, H.; Okamoto, S. *Appl. Phys. Lett.* **1997**, *71*, 2563–2565.
(71) Cahen, D.; Kahn, A. *Adv. Mater.* **2003**, *15*, 271–277.
(72) Marsi, M.; Houdre, R.; Rudra, A.; Ilegems, M.; Gozzo, F.; Coluzza, C.; Margaritondo, G. *Phys. Rev. B* **1993**, *47*, 6455–6459.
(73) Kronik, L.; Shapira, Y. *Surf. Sci. Rep.* **1999**, *37*, 1–206.
(74) Grobosch, M.; Knupfer, M. *Adv. Mater.* **2007**, *19*, 754–756.
(75) Lang, N. D.; Kohn, W. *Phys. Rev. B* **1971**, *3*, 1215–1223.
(76) Lang, N. D. *Phys. Rev. Lett.* **1981**, *46*, 842–845.
(77) Bagus, P. S.; Staemmler, V.; Woll, C. *Phys. Rev. Lett.* **2002**, *89*, 096104/1–4.
(78) Witte, G.; Lukas, S.; Bagus, P. S.; Wöll, C. *Appl. Phys. Lett.* **2005**, *87*, 263502/1–3.
(79) Fukagawa, H.; Kera, S.; Kataoka, T.; Hosoumi, S.; Watanabe, Y.; Kudo, K.; Ueno, N. *Adv. Mater.* **2007**, *19*, 665–668.
(80) Koch, N.; Vollmer, A. *Appl. Phys. Lett.* **2006**, *89*, 162107/1–3.
(81) Tengstedt, C.; Osikowicz, W.; Salaneck, W. R.; Parker, I. D.; Hsu, C. H.; Fahlman, M. *Appl. Phys. Lett.* **2006**, *88*, 053502/1–3.
(82) Braun, S.; Osikowicz, W.; Wang, Y.; Salaneck, W. R. *Org. Electron.* **2007**, *8*, 14–20.
(83) Fahlman, M.; Crispin, A.; Crispin, X.; Henze, S. K. M.; de Jong, M. P.; Osikowicz, W.; Tengstedt, C.; Salaneck, W. R. *J. Phys.: Condens. Matter* **2007**, *19*, 183202/1–20.
(84) Crispin, A.; Crispin, X.; Fahlman, M.; Berggren, M.; Salaneck, W. R. *Appl. Phys. Lett.* **2006**, *89*, 213503/1–3.
(85) Duhm, S.; Glowatzki, H.; Rabe, J. P.; Koch, N.; Johnson, R. L. *Appl. Phys. Lett.* **2007**, *90*, 122113/1–3.
(86) Sueyoshi, T.; Fukagawa, H.; Ono, M.; Kera, S.; Ueno, N. *Appl. Phys. Lett.* **2009**, *95*, 183303/1–3.
(87) Vázquez, H.; Flores, F.; Oszwaldowski, R.; Ortega, J.; Pérez, R.; Kahn, A. *Appl. Surf. Sci.* **2004**, *234*, 107–112.
(88) Vázquez, H.; Oszwaldowski, R.; Pou, P.; Ortega, J.; Pérez, R.; Flores, F.; Kahn, A. *Europhys. Lett.* **2004**, *65*, 802–808.
(89) Vázquez, H.; Gao, W.; Flores, F.; Kahn, A. *Phys. Rev. B* **2005**, *71*, 041306/1–4.
(90) Kahn, A.; Zhao, W.; Gao, W. Y.; Vázquez, H.; Flores, F. *Chem. Phys.* **2006**, *325*, 129–137.
(91) Vázquez, H.; Flores, F.; Kahn, A. *Org. Electron.* **2007**, *8*, 241–248.
(92) Vázquez, H.; Dappe, Y. J.; Ortega, J.; Flores, F. *J. Chem. Phys.* **2007**, *126*, 144703/1–8.
(93) Vázquez, H.; Dappe, Y. J.; Ortega, J.; Flores, F. *Appl. Surf. Sci.* **2007**, *254*, 378–382.
(94) Flores, F.; Ortega, J.; Vázquez, H. *Phys. Chem. Chem. Phys.* **2009**, *11*, 8658–8675.
(95) Tsiper, E. V.; Soos, Z. G.; Gao, W.; Kahn, A. *Chem. Phys. Lett.* **2002**, *360*, 47–52.
(96) Neaton, J. B.; Hybertsen, M. S.; Louie, S. G. *Phys. Rev. Lett.* **2006**, *97*, 216405/1–4.
(97) Amy, F.; Chan, C.; Kahn, A. *Org. Electron.* **2005**, *6*, 85–91.
(98) Hill, I. G.; Makinen, A. J.; Kafafi, Z. H. *J. Appl. Phys.* **2000**, *88*, 889–895.
(99) Sato, N.; Inokuchi, H.; Silinsh, E. A. *Chem. Phys.* **1987**, *115*, 269–277.
(100) Sato, N.; Seki, K.; Inokuchi, H. *J. Chem. Soc., Faraday Trans. 2* **1981**, *77*, 1621–1633.
(101) Seki, K. *Mol. Cryst. Liq. Cryst.* **1989**, *171*, 255–270.
(102) Tsiper, E. V.; Soos, Z. G. *Phys. Rev. B* **2001**, *64*, 195124/1–12.
(103) Tsiper, E. V.; Soos, Z. G. *Phys. Rev. B* **2003**, *68*, 085301/1–10.
(104) Verlaak, S.; Heremans, P. *Phys. Rev. B* **2007**, *75*, 115127/1–14.
(105) Norton, J. E.; Brédas, J. L. *J. Am. Chem. Soc.* **2008**, *130*, 12377–12384.
(106) Verlaak, S.; Beljonne, D.; Cheyns, D.; Rolin, C.; Linares, M.; Castet, F.; Cornil, J.; Heremans, P. *Adv. Funct. Mater.* **2009**, *19*, 3809–3814.
(107) Ueno, N.; Kera, S. *Prog. Surf. Sci.* **2008**, *83*, 490–557.
(108) Guaino, P.; Carty, D.; Hughes, G.; McDonald, O.; Cafolla, A. A. *Appl. Phys. Lett.* **2004**, *85*, 2777–2779.
(109) Söhnchen, S.; Lukas, S.; Witte, G. *J. Chem. Phys.* **2004**, *121*, 525–534.
(110) Wong, S. L.; Huang, H.; Huang, Y. L.; Wang, Y. Z.; Gao, X. Y.; Suzuki, T.; Chen, W.; Wee, A. T. S. *J. Phys. Chem. C* **2010**, *114*, 9356–9361.
(111) Käfer, D.; Ruppel, L.; Witte, G. *Phys. Rev. B* **2007**, *75*, 085309/1–14.
(112) France, C. B.; Schroeder, P. G.; Forsythe, J. C.; Parkinson, B. A. *Langmuir* **2003**, *19*, 1274–1281.
(113) France, C. B.; Schroeder, P. G.; Parkinson, B. A. *Nano Lett.* **2002**, *2*, 693–696.
(114) Schroeder, P. G.; France, C. B.; Park, J. B.; Parkinson, B. A. *J. Appl. Phys.* **2002**, *91*, 3010–3014.
(115) Kang, J. H.; Zhu, X. Y. *Appl. Phys. Lett.* **2003**, *82*, 3248–3250.
(116) Koch, N.; Vollmer, A.; Duhm, S.; Sakamoto, Y.; Suzuki, T. *Adv. Mater.* **2007**, *19*, 112–116.
(117) Salzmann, I.; Duhm, S.; Heimel, G.; Oehzelt, M.; Kniprath, R.; Johnson, R. L.; Rabe, J. P.; Koch, N. *J. Am. Chem. Soc.* **2008**, *130*, 12870–12871.
(118) Schiefer, S.; Huth, M.; Dobrinevski, A.; Nickel, B. *J. Am. Chem. Soc.* **2007**, *129*, 10316–10317.
(119) Nabok, D.; Puschnig, P.; Ambrosch-Draxl, C.; Werzer, O.; Resel, R.; Smilgies, D. M. *Phys. Rev. B* **2007**, *76*, 235322.
(120) Duhm, S.; Salzmann, I.; Heimel, G.; Oehzelt, M.; Haase, A.; Johnson, R. L.; Rabe, J. P.; Koch, N. *Appl. Phys. Lett.* **2009**, *94*, 033304/1–3.
(121) Ruiz, R.; Mayer, A. C.; Malliaras, G. G.; Nickel, B.; Scoles, G.; Kazimirov, A.; Kim, H.; Headrick, R. L.; Islam, Z. *Appl. Phys. Lett.* **2004**, *85*, 4926–4928.
(122) Salzmann, I.; Opitz, R.; Rogaschewski, S.; Rabe, J. P.; Koch, N.; Nickel, B. *Phys. Rev. B* **2007**, *75*, 174108/1–10.
(123) Duhm, S.; Glowatzki, H.; Rabe, J. P.; Koch, N.; Johnson, R. L. *Appl. Phys. Lett.* **2006**, *88*, 203109/1–3.
(124) Duhm, S.; Heimel, G.; Salzmann, I.; Glowatzki, H.; Johnson, R. L.; Vollmer, A.; Rabe, J. P.; Koch, N. *Nat. Mater.* **2008**, *7*, 326–332.
(125) Duhm, S.; Salzmann, I.; Koch, N.; Fukagawa, H.; Kataoka, T.; Hosoumi, S.; Nebashi, K.; Kera, S.; Ueno, N. *J. Appl. Phys.* **2008**, *104*, 033717/1–7.

(126) Ivanco, J.; Haber, T.; Krenn, J. R.; Netzer, F. P.; Resel, R.; Ramsey, M. G. *Surf. Sci.* **2007**, *601*, 178–187.
(127) Ivanco, J.; Krenn, J. R.; Ramsey, M. G.; Netzer, F. P.; Haber, T.; Resel, R.; Haase, A.; Stadlober, B.; Jakopic, G. *J. Appl. Phys.* **2004**, *96*, 2716–2724.
(128) Ivanco, J.; Netzer, F. P.; Ramsey, M. G. *J. Appl. Phys.* **2007**, *101*, 103712/1–7.
(129) Friedlein, R.; Crispin, X.; Pickholz, M.; Keil, M.; Stafström, S.; Salaneck, W. R. *Chem. Phys. Lett.* **2002**, *354*, 389–394.
(130) Chen, W.; Huang, H.; Chen, S.; Huang, Y. L.; Gao, X. Y.; Wee, A. T. S. *Chem. Mater.* **2008**, *20*, 7017–7021.
(131) Chen, W.; Qi, D. C.; Huang, Y. L.; Huang, H.; Wang, Y. Z.; Chen, S.; Gao, X. Y.; Wee, A. T. S. *J. Phys. Chem. C* **2009**, *113*, 12832–12839.
(132) Chen, W.; Chen, S.; Chen, S.; Huang, Y. L.; Huang, H.; Qi, D. C.; Gao, X. Y.; Ma, J.; Wee, A. T. S. *J. Appl. Phys.* **2009**, *106*, 064910/1–4.
(133) Chen, W.; Chen, S.; Huang, H.; Qi, D. C.; Gao, X. Y.; Wee, A. T. S. *Appl. Phys. Lett.* **2008**, *92*, 063308/1–3.
(134) Duhm, S.; Hosoumi, S.; Salzmann, I.; Gerlach, A.; Oehzelt, M.; Wedl, B.; Lee, T. L.; Schreiber, F.; Koch, N.; Ueno, N.; Kera, S. *Phys. Rev. B* **2010**, *81*, 045418/1–6.
(135) Heimel, G.; Salzmann, I.; Duhm, S.; Rabe, J. P.; Koch, N. *Adv. Funct. Mater.* **2009**, *19*, 3874–3879.
(136) Koch, N.; Gerlach, A.; Duhm, S.; Glowatzki, H.; Heimel, G.; Vollmer, A.; Sakamoto, Y.; Suzuki, T.; Zegenhagen, J.; Rabe, J. P.; Schreiber, F. *J. Am. Chem. Soc.* **2008**, *130*, 7300–7304.
(137) de Oteyza, D. G.; Wakayama, Y.; Liu, X.; Yang, W.; Cook, P. L.; Himpsel, F. J.; Ortega, J. E. *Chem. Phys. Lett.* **2010**, *490*, 54–57.
(138) Inoue, Y.; Sakamoto, Y.; Suzuki, T.; Kobayashi, M.; Gao, Y.; Tokito, S. *Jpn. J. Appl. Phys.* **2005**, *44*, 3663–3668.
(139) Sakamoto, Y.; Suzuki, T.; Kobayashi, M.; Gao, Y.; Fukai, Y.; Inoue, Y.; Sato, F.; Tokito, S. *J. Am. Chem. Soc.* **2004**, *126*, 8138–8140.
(140) Sakamoto, Y.; Suzuki, T.; Kobayashi, M.; Gao, Y.; Inoue, Y.; Tokito, S. *Mol. Cryst. Liq. Cryst.* **2006**, *444*, 225–232.
(141) Salzmann, I.; Duhm, S.; Heimel, G.; Rabe, J. P.; Koch, N.; Oehzelt, M.; Sakamoto, Y.; Suzuki, T. *Langmuir* **2008**, *24*, 7294–7298.
(142) Kowarik, S.; Gerlach, A.; Hinderhofer, A.; Milita, S.; Borgatti, F.; Zontone, F.; Suzuki, T.; Biscarini, F.; Schreiber, F. *Phys. Status Solidi (RRL)* **2008**, *2*, 120–122.
(143) Coropceanu, V.; Malagoli, M.; da Silva Filho, D. A.; Gruhn, N. E.; Bill, T. G.; Brédas, J. L. *Phys. Rev. Lett.* **2002**, *89*, 275503/1–4.
(144) Delgado, M. C. R.; Pigg, K. R.; da Silva Filho, D. A.; Gruhn, N. E.; Sakamoto, Y.; Suzuki, T.; Osuna, R. M.; Casado, J.; Hernández, V.; Navarrete, J. T. L.; Martinelli, N. G.; Cornil, J.; Sánchez-Carrera, R. S.; Coropceanu, V.; Brédas, J. L. *J. Am. Chem. Soc.* **2009**, *131*, 1502–1512.
(145) Vogel, J. O.; Salzmann, I.; Duhm, S.; Oehzelt, M.; Rabe, J. P.; Koch, N. *J. Mater. Chem.* **2010**, *20*, 4055–4066.
(146) Vogel, J. O.; Salzmann, I.; Opitz, R.; Duhm, S.; Nickel, B.; Rabe, J. P.; Koch, N. *J. Phys. Chem. B* **2007**, *111*, 14097–14101.
(147) Mitschke, U.; Bäuerle, P. *J. Mater. Chem.* **2000**, *10*, 1471–1507.
(148) Akcelrud, L. *Prog. Polym. Sci.* **2003**, *28*, 875–962.
(149) McCullough, R. D.; Tristram-Nagle, S.; Williams, S. P.; Lowe, R. D.; Jayaraman, M. *J. Am. Chem. Soc.* **1993**, *115*, 4910–4911.
(150) Winokur, M. J.; Spiegel, D.; Kim, Y.; Hotta, S.; Heeger, A. J. *Synth. Met.* **1989**, *28*, C419–C426.
(151) Prosa, T. J.; Winokur, M. J.; Moulton, J.; Smith, P.; Heeger, A. J. *Macromolecules* **1992**, *25*, 4364–4372.
(152) Luzny, W.; Trznadel, M.; Pron, A. *Synth. Met.* **1996**, *81*, 71–74.
(153) Yang, C. Y.; Soci, C.; Moses, D.; Heeger, A. J. *Synth. Met.* **2005**, *155*, 639–642.
(154) Kline, R. J.; McGehee, M. D.; Toney, M. F. *Nat. Mater.* **2006**, *5*, 222–228.
(155) Sirringhaus, H.; Brown, P. J.; Friend, R. H.; Nielsen, M. M.; Bechgaard, K.; Langeveld-Voss, B. M. W.; Spiering, A. J. H.; Janssen, R. A. J.; Meijer, E. W.; Herwig, P.; de Leeuw, D. M. *Nature* **1999**, *401*, 685–688.
(156) Yang, H. C.; Shin, T. J.; Bao, Z. N.; Ryu, C. Y. *J. Polym. Sci., Part B* **2007**, *45*, 1303–1312.
(157) Yang, H. H.; LeFevre, S. W.; Ryu, C. Y.; Bao, Z. N. *Appl. Phys. Lett.* **2007**, *90*, 172116/1–3.
(158) Yang, H. C.; Shin, T. J.; Yang, L.; Cho, K.; Ryu, C. Y.; Bao, Z. N. *Adv. Funct. Mater.* **2005**, *15*, 671–676.
(159) Hugger, S.; Thomann, R.; Heinzel, T.; Thurn-Albrecht, T. *Colloid Polym. Sci.* **2004**, *282*, 932–938.
(160) Kim, Y.; Cook, S.; Tuladhar, S. M.; Choulis, S. A.; Nelson, J.; Durrant, J. R.; Bradley, D. D. C.; Giles, M.; McCulloch, I.; Ha, C. S.; Ree, M. *Nat. Mater.* **2006**, *5*, 197–203.
(161) Aasmundtveit, K. E.; Samuelsen, E. J.; Guldstein, M.; Steinsland, C.; Flornes, O.; Fagermo, C.; Seeberg, T. M.; Pettersson, L. A. A.; Inganas, O.; Feidenhans'l, R.; Ferrer, S. *Macromolecules* **2000**, *33*, 3120–3127.
(162) Sandberg, H. G. O.; Frey, G. L.; Shkunov, M. N.; Sirringhaus, H.; Friend, R. H.; Nielsen, M. M.; Kumpf, C. *Langmuir* **2002**, *18*, 10176–10182.
(163) Wang, G. M.; Swensen, J.; Moses, D.; Heeger, A. J. *J. Appl. Phys.* **2003**, *93*, 6137–6141.
(164) Chang, J. F.; Sun, B. Q.; Breiby, D. W.; Nielsen, M. M.; Solling, T. I.; Giles, M.; McCulloch, I.; Sirringhaus, H. *Chem. Mater.* **2004**, *16*, 4772–4776.
(165) Joshi, S.; Grigorian, S.; Pietsch, U.; Pingel, P.; Zen, A.; Neher, D.; Scherf, U. *Macromolecules* **2008**, *41*, 6800–6808.
(166) Kline, R. J.; McGehee, M. D.; Kadnikova, E. N.; Liu, J. S.; Frechet, J. M. J.; Toney, M. F. *Macromolecules* **2005**, *38*, 3312–3319.
(167) Zen, A.; Pflaum, J.; Hirschmann, S.; Zhuang, W.; Jaiser, F.; Asawapirom, U.; Rabe, J. P.; Scherf, U.; Neher, D. *Adv. Funct. Mater.* **2004**, *14*, 757–764.
(168) Joshi, S.; Grigorian, S.; Pietsch, U. *Phys. Status Solidi A* **2008**, *205*, 488–496.
(169) Zen, A.; Saphiannikova, M.; Neher, D.; Grenzer, J.; Grigorian, S.; Pietsch, U.; Asawapirom, U.; Janietz, S.; Scherf, U.; Lieberwirth, I.; Wegner, G. *Macromolecules* **2006**, *39*, 2162–2171.
(170) Meille, S. V.; Romita, V.; Caronna, T.; Lovinger, A. J.; Catellani, M.; Belobrzeckaja, L. *Macromolecules* **1997**, *30*, 7898–7905.
(171) Kline, R. J.; McGehee, M. D.; Kadnikova, E. N.; Liu, J. S.; Frechet, J. M. J. *Adv. Mater.* **2003**, *15*, 1519–1522.
(172) Kim, D. H.; Jang, Y.; Park, Y. D.; Cho, K. *Langmuir* **2005**, *21*, 3203–3206.
(173) Hao, X. T.; Hosokai, T.; Mitsuo, N.; Kera, S.; Okudaira, K. K.; Mase, K.; Ueno, N. *J. Phys. Chem. B* **2007**, *111*, 10365–10372.
(174) DeLongchamp, D. M.; Vogel, B. M.; Jung, Y.; Gurau, M. C.; Richter, C. A.; Kirillov, O. A.; Obrzut, J.; Fischer, D. A.; Sambasivan, S.; Richter, L. J.; Lin, E. K. *Chem. Mater.* **2005**, *17*, 5610–5612.
(175) Hao, X. T.; Hosokai, T.; Mitsuo, N.; Kera, S.; Mase, K.; Okudaira, K. K.; Ueno, N. *Appl. Phys. Lett.* **2006**, *89*, 182113/1–3.
(176) Ho, P. K. H.; Chua, L. L.; Dipankar, M.; Gao, X. Y.; Qi, D. C.; Wee, A. T. S.; Chang, J. F.; Friend, R. H. *Adv. Mater.* **2007**, *19*, 215–221.
(177) Kanai, K.; Miyazaki, T.; Suzuki, H.; Inaba, M.; Ouchi, Y.; Seki, K. *Phys. Chem. Chem. Phys.* **2010**, *12*, 273–282.
(178) Zhang, F.; Vollmer, A.; Zhang, J.; Xu, Z.; Rabe, J. P.; Koch, N. *Org. Electron.* **2007**, *8*, 606–614.
(179) Lyon, J. E.; Cascio, A. J.; Beerbom, M. M.; Schlaf, R.; Zhu, Y.; Jenekhe, S. A. *Appl. Phys. Lett.* **2006**, *88*, 222109/1–3.
(180) Cascio, A. J.; Lyon, J. E.; Beerbom, M. M.; Schlaf, R.; Zhu, Y.; Jenekhe, S. A. *Appl. Phys. Lett.* **2006**, *88*, 062104/1–3.
(181) Yi, Y.; Lyon, J. E.; Beerbom, M. M.; Schlaf, R. *J. Appl. Phys.* **2006**, *100*, 093719/1–7.
(182) Osikowicz, W.; de Jong, M. P.; Braun, S.; Tengstedt, C.; Fahlman, M.; Salaneck, W. R. *Appl. Phys. Lett.* **2006**, *88*, 193504/1–3.
(183) Ke, L.; Chua, S. J.; Zhang, K.; Yakovlev, N. *Appl. Phys. Lett.* **2002**, *80*, 2195–2197.
(184) Aziz, H.; Popovic, Z.; Tripp, C. P.; Hu, N. X.; Hor, A. M.; Xu, G. *Appl. Phys. Lett.* **1998**, *72*, 2642–2644.
(185) Aziz, H.; Popovic, Z.; Xie, S.; Hor, A. M.; Hu, N. X.; Tripp, C.; Xu, G. *Appl. Phys. Lett.* **1998**, *72*, 756–758.
(186) Melpignano, P.; Baron-Toaldo, A.; Biondo, V.; Priante, S.; Zamboni, R.; Murgia, M.; Caria, S.; Gregoratti, L.; Barinov, A.; Kiskinova, M. *Appl. Phys. Lett.* **2005**, *86*, 041105/1–3.
(187) Burrows, P. E.; Bulovic, V.; Forrest, S. R.; Sapochak, L. S.; Mccarty, D. M.; Thompson, M. E. *Appl. Phys. Lett.* **1994**, *65*, 2922–2924.
(188) Kim, S. Y.; Kim, K. Y.; Tak, Y. H.; Lee, J. L. *Appl. Phys. Lett.* **2006**, *89*, 132108/1–3.
(189) Garnier, F.; Yassar, A.; Hajlaoui, R.; Horowitz, G.; Deloffre, F.; Servet, B.; Ries, S.; Alnot, P. *J. Am. Chem. Soc.* **1993**, *115*, 8716–8721.
(190) Horowitz, G.; Garnier, F.; Yassar, A.; Hajlaoui, R.; Kouki, F. *Adv. Mater.* **1996**, *8*, 52–54.
(191) Torsi, L.; Dodabalapur, A.; Rothberg, L. J.; Fung, A. W. P.; Katz, H. E. *Science* **1996**, *272*, 1462–1464.
(192) Dimitrakopoulos, C. D.; Purushothaman, S.; Kymissis, J.; Callegari, A.; Shaw, J. M. *Science* **1999**, *283*, 822–824.
(193) Halik, M.; Klauk, H.; Zschieschang, U.; Schmid, G.; Ponomarenko, S.; Kirchmeyer, S.; Weber, W. *Adv. Mater.* **2003**, *15*, 917–922.
(194) Chua, L. L.; Zaumseil, J.; Chang, J. F.; Ou, E. C.-W.; Ho, P. K.-H.; Sirringhaus, H.; Friend, R. H. *Nature* **2005**, *434*, 194–199.
(195) Newman, C. R.; Frisbie, C. D.; da Silva Filho, D. A.; Brédas, J. L.; Ewbank, P. C.; Mann, K. R. *Chem. Mater.* **2004**, *16*, 4436–4451.
(196) Dodabalapur, A.; Katz, H. E.; Torsi, L.; Haddon, R. C. *Science* **1995**, *269*, 1560–1562.
(197) Klauk, H.; Zschieschang, U.; Pflaum, J.; Halik, M. *Nature* **2007**, *445*, 745–748.
(198) Wen, Y. G.; Liu, Y. Q. *Adv. Mater.* **2010**, *22*, 1331–1345.
(199) Cai, X. Y.; Burand, M. W.; Newman, C. R.; da Silva Filho, D. A.; Pappenfus, T. M.; Bader, M. M.; Brédas, J. L.; Mann, K. R.; Frisbie, C. D. *J. Phys. Chem. B* **2006**, *110*, 14590–14597.
(200) Kono, T.; Kumaki, D.; Nishida, J.; Sakanoue, T.; Kakita, M.; Tada, H.; Tokito, S.; Yamashita, Y. *Chem. Mater.* **2007**, *19*, 1218–1220.
(201) Chen, H. Z.; Ling, M. M.; Mo, X.; Shi, M. M.; Wang, M.; Bao, Z. *Chem. Mater.* **2007**, *19*, 816–824.
(202) Mamada, M.; Nishida, J. I.; Kumaki, D.; Tokito, S.; Yamashita, Y. *Chem. Mater.* **2007**, *19*, 5404–5409.
(203) Jung, B. J.; Sun, J.; Lee, T.; Sarjeant, A.; Katz, H. E. *Chem. Mater.* **2009**, *21*, 94–101.
(204) Naraso; Nishida, J.; Kumaki, D.; Tokito, S.; Yamashita, Y. *J. Am. Chem. Soc.* **2006**, *128*, 9598–9599.

(205) Facchetti, A.; Deng, Y.; Wang, A. C.; Koide, Y.; Sirringhaus, H.; Marks, T. J.; Friend, R. H. *Angew. Chem., Int. Ed.* **2000**, *39*, 4547–4551.
(206) Yoon, M. H.; Facchetti, A.; Stern, C. E.; Marks, T. J. *J. Am. Chem. Soc.* **2006**, *128*, 5792–5801.
(207) Nakagawa, T.; Kumaki, D.; Nishida, J. I.; Tokito, S.; Yamashita, Y. *Chem. Mater.* **2008**, *20*, 2615–2617.
(208) Ando, S.; Nishida, J.; Fujiwara, E.; Tada, H.; Inoue, Y.; Tokito, S.; Yamashita, Y. *Chem. Mater.* **2005**, *17*, 1261–1264.
(209) Facchetti, A.; Mushrush, M.; Yoon, M. H.; Hutchison, G. R.; Ratner, M. A.; Marks, T. J. *J. Am. Chem. Soc.* **2004**, *126*, 13859–13874.
(210) Dholakia, G. R.; Meyyappan, M.; Facchetti, A.; Marks, T. J. *Nano Lett.* **2006**, *6*, 2447–2455.
(211) Azumi, R.; Gotz, G.; Debaerdemaeker, T.; Bauerle, P. *Chem.—Eur. J.* **2000**, *6*, 735–744.
(212) Bröker, B.; Blum, R. P.; Frisch, J.; Vollmer, A.; Hofmann, O. T.; Rieger, R.; Müllen, K.; Rabe, J. P.; Zojer, E.; Koch, N. *Appl. Phys. Lett.* **2008**, *93*, 243303/1–3.
(213) Campbell, I. H.; Kress, J. D.; Martin, R. L.; Smith, D. L.; Barashkov, N. N.; Ferraris, J. P. *Appl. Phys. Lett.* **1997**, *71*, 3528–3530.
(214) Cheng, X. Y.; Noh, Y. Y.; Wang, J. P.; Tello, M.; Frisch, J.; Blum, R. P.; Vollmer, A.; Rabe, J. P.; Koch, N.; Sirringhaus, H. *Adv. Funct. Mater.* **2009**, *19*, 2407–2415.
(215) de Boer, B.; Hadipour, A.; Mandoc, M. M.; van Woudenbergh, T.; Blom, P. W. M. *Adv. Mater.* **2005**, *17*, 621–625.
(216) Ihm, K.; Kim, B.; Kang, T. H.; Kim, K. J.; Joo, M. H.; Kim, T. H.; Yoon, S. S.; Chung, S. *Appl. Phys. Lett.* **2006**, *89*, 033504/1–3.
(217) Koch, N.; Duhm, S.; Rabe, J. P.; Vollmer, A.; Johnson, R. L. *Phys. Rev. Lett.* **2005**, *95*, 237601/1–4.
(218) Lee, T. W.; Hsu, J. W. P. *Appl. Phys. Lett.* **2006**, *89*, 223511/1–3.
(219) Rentenberger, S.; Vollmer, A.; Zojer, E.; Schennach, R.; Koch, N. *J. Appl. Phys.* **2006**, *100*, 053701/1–6.
(220) Stadlober, B.; Haas, U.; Gold, H.; Haase, A.; Jakopic, G.; Leising, G.; Koch, N.; Rentenberger, S.; Zojer, E. *Adv. Funct. Mater.* **2007**, *17*, 2687–2692.